EARTH SCIENCES
RESEARCH JOURNAL

Earth Sci. Res. J. Vol. 22, No. 4 (December, 2018): 301-318

UNIVERSIDAD NACIONAL DE COLOMBIA

MINERALOGY

Characteristics of genetic mineralogy of pyrite and quartz and their indicating significance in the Gaosongshan Gold Deposit, Heilongjiang Province, NE China

Huiqing Geng[1,2], Xuexiang Gu[2], Yongmei Zhang[2]

[1] School of Resources, Hebei Geosciences University, Shijiazhuang 050031, China. qingqing_heb@126.com

[2] School of Earth Sciences and Resources, China University of Geosciences, Beijing 100083, China

ABSTRACT

The Gaosongshan epithermal gold deposit in Heilongjiang, Northeast China, is hosted by the Lower Cretaceous intermediate-basic volcanic rocks. Three auriferous quartz veins including eleven gold orebodies were all discovered in tectonoclastic zones. Genetic mineralogy study including the thermoelectricity, rare earth elements and trace elements of pyrite and rare earth elements of quartz were carried out. Thermoelectric conductive type of pyrite is mainly N-P type. Calculating the thermoelectric parameters X_{NP} and denudation percentage γ of pyrites from orebodies 1-I, 2-II and 2-IV, suggests that gold orebodies are all eroded to their middle-lower parts. The variable range of Co concentrations (51.3-264.0ppm) and Ni concentrations (68.9-258.0ppm) and Co: Ni ratio (0.31-1.90), together with relatively small Sr/Ba ratio in ore-bearing pyrites (0.11-0.50), supports a hydrothermal origin of mineralization at Gaosongshan gold deposit. Compared with volcanic rocks, the chondrite-normalized REE patterns of ore-bearing pyrites and quartz are all LREE enriched with similar ΣLREE/ΣHREE ratio ranging from 7.37-13.68 in ore-bearing pyrites, 4.74-15.37 in ore-bearing quartz and no Ce anomalies. δEu values in ore-bearing pyrites and quartz are 0.65-1.66 (average=0.93) and 0.66-1.62 (average=1.03), respectively. δEu values of volcanic rocks are 0.86-1.07 (average 0.94), suggesting no obvious negative Eu anomalies. Similar REE characteristics of ore-bearing pyrites and quartz and volcanic rocks, together with previous oxygen and hydrogen isotope studies of quartz, suggest that the ore-forming fluids of the Gaosongshan gold deposit were mainly magmatic origin which was associated with andesitic magma and was partly mixed with atmospheric water. Comparing trace elements characteristics of ore-bearing pyrites with volcanic rocks, together with previous S isotopic studies, it is concluded that the ore-forming materials were derived from the surrounding rocks. Slight changes of Y/Ho (23.80-27.28), Zr/Hf (35.41-47.83), Nb/Ta (10.96-18.52) in ore-bearing pyrites indicate that the ore-forming fluid system is relatively stable during the ore-forming process

Keywords: Pyrite; Quartz; Rare earth elements; Genetic mineralogy; Gaosongshan Gold Deposit; China.

Características de mineralogía genética de piritas y cuarzos y su importancia en el yacimiento aurífero de Gaosongshan, Provincia de Heilongjiang, al noreste de China

RESUMEN

El yacimiento aurífero epitermal de Gaosongshan en Heilongjiang, al noreste de China, está incrustado en una formación de rocas volcánicas en el Cretácico Inferior. Tres vetas de cuarzo aurífero que incluyen once yacimientos de oro se descubrieron en zonas tectonoclásticas. Se realizaron análisis de mineralogía genética, entre estos de termoelectricidad, de tierras raras, y de trazas de piritas y tierras raras. El tipo de conductividad termoeléctrica de la pirita es principalmente tipo N-P. El cálculo de los parámetros X_{NP} de termoelectricidad y el porcentaje de denudación γ de piritas en los yacimientos 1-I, 2-II y 2-IV sugiere que los yacimientos auríferos están erosionados en sus partes medias y bajas. El rango variable de las concentraciones de Co (51.3-264.0ppm) y de Ni (68.9-258.0ppm), y el índice Co: Ni (0.31-1.90), junto con un índice pequeño de Sr/Ba de piritas mineralizadas (0.11-0.50) suponen un origen hidrotérmico de mineralización en el yacimiento aurífero de Gaosongshan. Comparado con rocas volcánicas, los patrones de tierras raras en las condritas normalizadas de piritas y cuarzos son todos tierras raras ligeros enriquecidos con índices ΣLREE/ΣHREE similares y que se ubican en el rango 7.37-13.68 en las piritas mineralizadas, 4.74-15.37 en los cuarzos mineralizados y sin anomalías de Cerio. Los valores δEu en piritas mineralizadas y cuarzos son de 0.65-1.66 (con promedio de 0.93) y 0.66-1.62 (con promedio de 1.03), respectivamente. Los valores δEu de las rocas volcánicas son 0.861.07 (con promedio de 0.94), lo que sugiere que no hay anomalías negativas de europio. Las características similares de tierras raras entre piritas mineralizadas, cuarzos y rocas volcánicas, al igual que estudios previos de isotopos de oxígeno e hidrógeno en cuarzos, sugieren que los fluidos hidrotermales del yacimiento de Gaosongshan son principalmente de origen magmático, el cual está asociado con el magma andesítico, y está parcialmente mezclado con agua atmosférica.

Palabras clave: Piritas; cuarzos; tierras raras; mineralogía genética; yacimiento aurífero de Gaosongshan; China.

Record
Manuscript received: 22/05/2017
Accepted for publication: 27/07/2018

How to cite item
Geng, H., Gu, X., & Zhang, Y. (2018). Characteristics of genetic mineralogy of pyrite and quartz and their indicating significance in the Gaosongshan Gold Deposit, Heilongjiang Province, NE China. *Earth Sciences Research Journal*, 22(4), 301-318.
DOI: https://doi.org/10.15446/esrj.v22n4.57512

Al comparar las características de los elementos traza en las piritas mineralizadas con las rocas volcánicas, y basados en estudios isotópicos del azufre, se puede concluir que los materiales hidrotermales se derivan de las rocas circundantes. Pequeños cambios de las piritas mineralizadas en Y/Ho (23.8027.28), Zr/Hf (35.4147.83), Nb/Ta (10.96-1852) indican que el sistema hidrotermal del depósito es relativamente estabe durante los procesos hidrotérmicos.

Introduction

The epithermal deposit is originally defined by Lindgren (1933). After decades of research (Heald et al., 1987; Hedenquist and Lowenstern, 1994; Cooke and Simmons, 2000; Chen et al., 2001), the terminology epithermal is still used but its definition has been broadened. It is considered that epithermal deposits formed at relatively low temperatures (100-320°C) and shallow depths (surface to 1-2km) (White and Hedenquist 1995; Chen et al., 2012). According to their geological environments, altered minerals and fluid chemistry, the epithermal deposits can be classified into two types: low-sulfidation type and high-sulfidation type (Bonham, 1986; White and Hedenquist, 1990, 1995; Hedenquist et al., 1998; Hedenquist et al., 2000), also known as adularia-sericite type and alunite-kaolinite type, respectively (Heald et al., 1987; Arribas, 1995; Hedenquist et al., 1998). As one of important type of gold deposits in the world, epithermal gold deposits have provided more than 6000 tons of gold reserve (Kerrich et al., 2000), which are mainly located in the metallogenic domain of the Circum-Pacific, Mediterranean-Himalaya and paleo-Asian (Chen et al., 2001; Jiang et al., 2004; Sillitoe, 2008; Hao et al., 2016). Many deposits of this type developed in China's northeast region, which is not only one part of Pacific Rim metallogenic domain, but also one of paleo-Asian metallogenic domain. These deposits are mostly distributed in four ore concentrating districts: Derbugan, Huma, Lesser Hinggan Range, eastern part of Jilin (Qi et al., 2005). Gaosongshan deposit is a newly discovered large epithermal gold deposit which is located in the Lesser Hinggan Range ore concentrating district.

The electrical properties of pyrite have been studied since the beginning of the 19th century (Hill and Green, 1962; Zhao, 1990; Yan et al., 2012). As an important physical property, the thermoelectricity of pyrite has been widely applied in gold deposits research (Ying et al., 2001; Ji et al., 2013; Xue et al., 2014). The change rule of the conduction type and thermoelectric in the vertical direction is an important sign denoting the orebody denudation level (Li et al., 1996; Chen, 1987; Shao et al., 1990). With detailed genetic mineralogy data of pyrite, the prospects of gold deposits can get better evaluated.

Nowadays, trace elements and rare earth elements (REE) determinations of pyrites and quartz are carried out by different in situ techniques such as laser ablation-inductively coupled plasma-mass spectrometry (LA-ICP-MS), secondary ion mass spectrometry (SIMS) and electron probe microanalysis (EPMA). As one of the most sensitive methods, inductively coupled plasma mass spectrometry (ICP-MS) has been widely utilized in recent years (Date and Gray, 1985; Lichte et al., 1987; Kantipuly and Westland, 1988; Liu, 1995; Fan et al., 2000; Ghazi et al., 1993; Su et al., 1998; Bie et al., 2000; Li et al., 2003; Li et al., 2004). The trace elements and the REEs are valuable in identifying the source of ore-forming materials and fluid, tracing the evolution of hydrothermal systems, constraining the conditions of ore formation, and evaluating the genesis of ore deposits (Dennen, 1967; Henderson, 1984; Michard and Albarède, 1986; Shao, 1988; Lottermoser, 1992; Klinkhammer et al., 1994; Franchini et al., 2015).

Previous studies about the Gaosongshan gold deposit focusing on metallogenic geological conditions, the origin of metallogenic materials, petrology and geochemistry of ore-bearing volcanic rocks, diagenetic tectonic setting, gold enrichment mechanism and geochemical studies of primary halos, have been published (Lv, 2012; Wang et al., 2014; Zheng et al., 2014; Hao et al., 2014; Hao et al., 2016). No work about the thermoelectric properties of pyrites, REE characteristics of pyrites and quartz and their significant geological significance has yet been published in English. In this study, new REE data of pyrites and quartz from the Gaosongshan gold deposit, analyzed with ICP-MS, are presented to further constrain the source of hydrothermal fluid and ore-forming materials. Measured with BHTE-08 thermoelectric coefficient instrument, the thermoelectric properties of pyrites are analyzed to provide information about the orebody denudation level and the medium conditions during the formation of deposits, and thus giving suggestions on finding blind orebodies.

Regional geology

The Gaosongshan gold deposit is located in the northeastern part of the East Xingmeng Orogenic Belt (EXOB) in NE China (Fig. 1a). The EXOB, which is separated from the North China Craton by the Chifeng-Kaiyuan fault, located between the Siberian and the North China Craton, comprises a series of micro-continents (Sengör et al., 1993; Zeng et al., 2012; Ouyang et al., 2013): the Eerguna block in the northeast, the Xing'an and Songliao blocks in the center, the Liaoyuan terrane in the southeast and the Jiamusi block in the East, which is separated from the Songliao block by the Mudanjiang fault. Tectonism and magmatism in this area were controlled by the evolution of the Paleo-Asian Ocean in the Paleozoic. Final closure of the Paleo-Asian Ocean which is characterized by suturing between the Songliao block and the Liaoyuan block is believed to have taken place along the Solonker-Xar Moron-Changchun suture zone during the Late Permian to the Early Triassic (Wu et al., 2011; Ouyang et al., 2013).

According to previous works (e.g., Zhou et al., 2009; Wilde et al., 2010; Zhang et al., 2010), the exposed stratigraphy in this study area comprises Precambrian metamorphic basement, Cambrian and Permian submarine sedimentary cover, Jurassic to Cretaceous terrigenous clastic and volcanic rocks and Cenozoic clastic rocks and basalt. The Precambrian metamorphic rocks are composed of gold-bearing silicon-iron formation from the Dongfengshan group and schist from the Heilongjiang Group. Cambrian rocks consist of dolomite, dolomite limestone and marble, unconformably overlying the Precambrian metamorphic rocks. Permian metamorphic clastic rocks comprise metasandstone, slate and phyllite, which discordantly overlie the Cambrian strata. Meanwhile, the Permian strata are discordantly overlain by the Jurassic terrigenous clastic rocks, consisting of sandstone and sandy conglomerate. The Cretaceous volcanic rocks, widely distributed throughout this area, are composed of basalt, trachyandesite, andesite, tuff, rhyolite and rhyolitic tuff. The Oligocene clast rocks and the Quaternary unconsolidated sediment are also extensively distributed in this study area.

Complex geological evolution from the Early Jurassic has resulted in extensive precious and nonferrous metal mineralization in this area, especially epithermal gold mineralization. A number of deposits including Gaosongshan, Dong'an, and Tuanjiegou (Zhou et al., 2002; Zhang et al., 2010; Liu et al., 2015; Hao et al., 2016; Wang et al., 2016;) have been discovered in recent years in Heilongjiang Province. The oldest formations in this area are Proterozoic greenschist facies metamorphic rocks of the Heilongjiang Group. Gold mineralization was controlled by many faults and its secondary faults. Major structures are dominated by the NW-SE-trending Shaaqi fault and a number of associated fractures trending NEE, NWW and EW (Fig. 1c).

Deposit geology

Strata

The Gaosongshan gold deposit, one of the epithermal gold deposits in Heilongjiang Province, discovered in 2000, is located in the northern part of the Yichun-Yanshou fold belt, which is situated between the Xing'an-Songnen block and the Jiamusi block (Wilde et al., 2010; Zhou et al., 2010) (Fig. 1b). The strata exposed are mainly intermediate-basic volcanic rocks, consist of the Lower Cretaceous Banzifang Formation (K1b) and the Ningyuancun Formation (K1n) (Fig. 2), hosting the mineralization at

Gaosongshan gold deposit. The Banzifang Formation, the main wall rock of veins I and II, is widespread in this area and consists of andesite, basaltic andesite, dacite, trachyandesite, andesitic volcanic breccia, and tufflava. The Ningyuancun Formation, the major host rock of vein III, is composed of tuff, rhyolite, and volcaniclastic rock.

Magmatic rocks

Although the scale of intrusive rocks in this area is relatively small, the types of intrusive rocks are complex, mainly intermediate-acid rocks. Granite and alaskite from the Late Variscan, located in the southern and eastern of the mining area, mainly occur as batholite or stock. Biotite granite, granodiorite and granite porphyry from the Early Yanshanian, distributed in the eastern part of the mining area, occur as batholite, stock or minor intrusive bodies.

Structure

There are many well-developed fault structures, such as the Shaaqi fracture, providing channels for ore solutions, which is NW-SE trending, and its associated fracture, the main host structure, trending NEE, NWW or EW (Fig. 2). The Wuqiganxiao-Gaosongshan fault and Xueshuiwen fault are NE-trending extensional structures controlling the emplacement of Early Mesozoic magmatic rocks and the deposition of Mesozoic volcanic rocks (Fig. 1c).

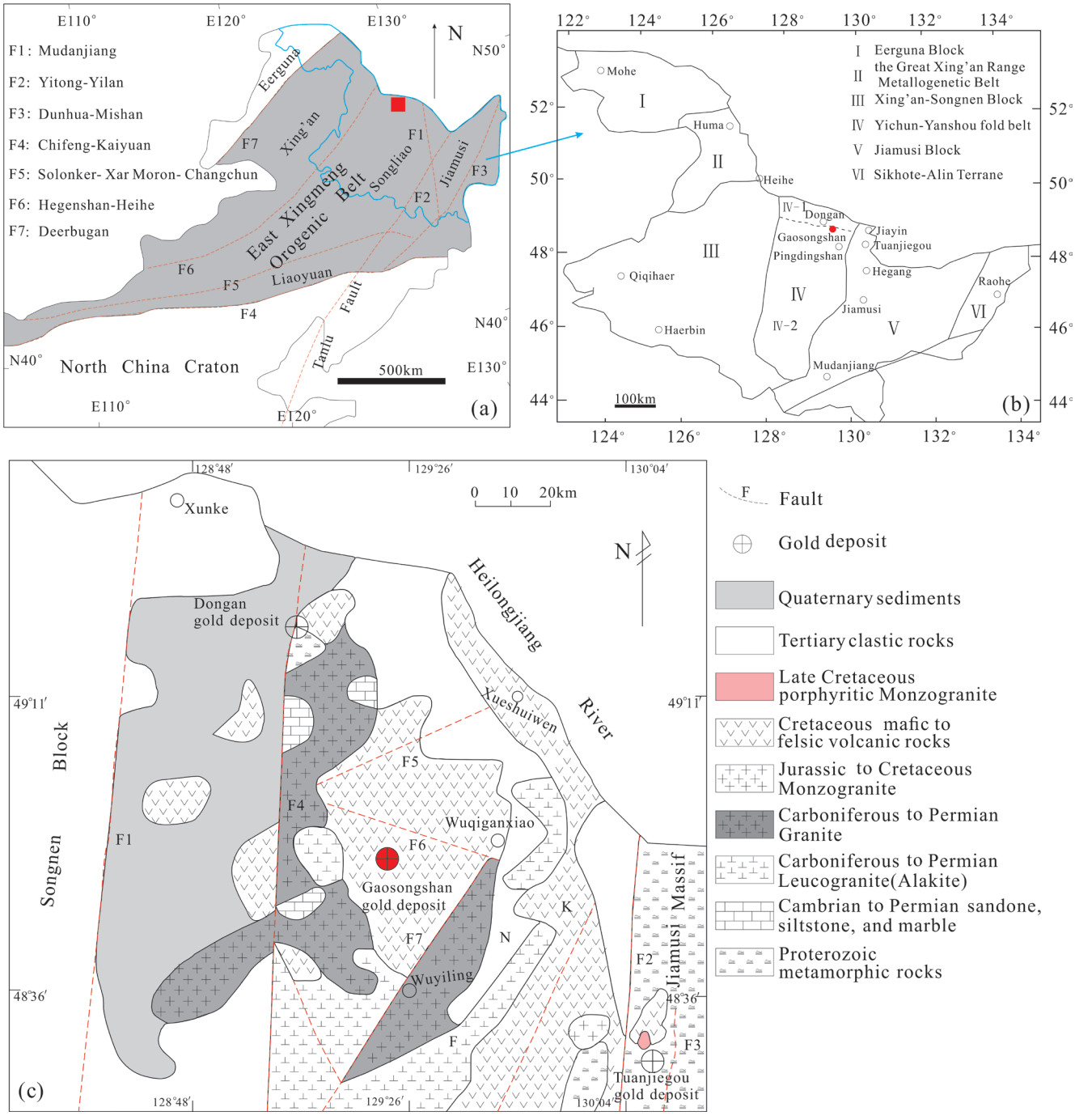

Figure 1. (a) Tectonic framework of northeastern China (modified from Wu et al., 2000; Wu et al., 2011; IMBGMR, 1991). (b) The distribution of the gold deposits in Heilongjiang Province (after HBGMR, 1993). (c) Regional geological map of the Gaosongshan gold deposit (modified after Hao et al., 2016)

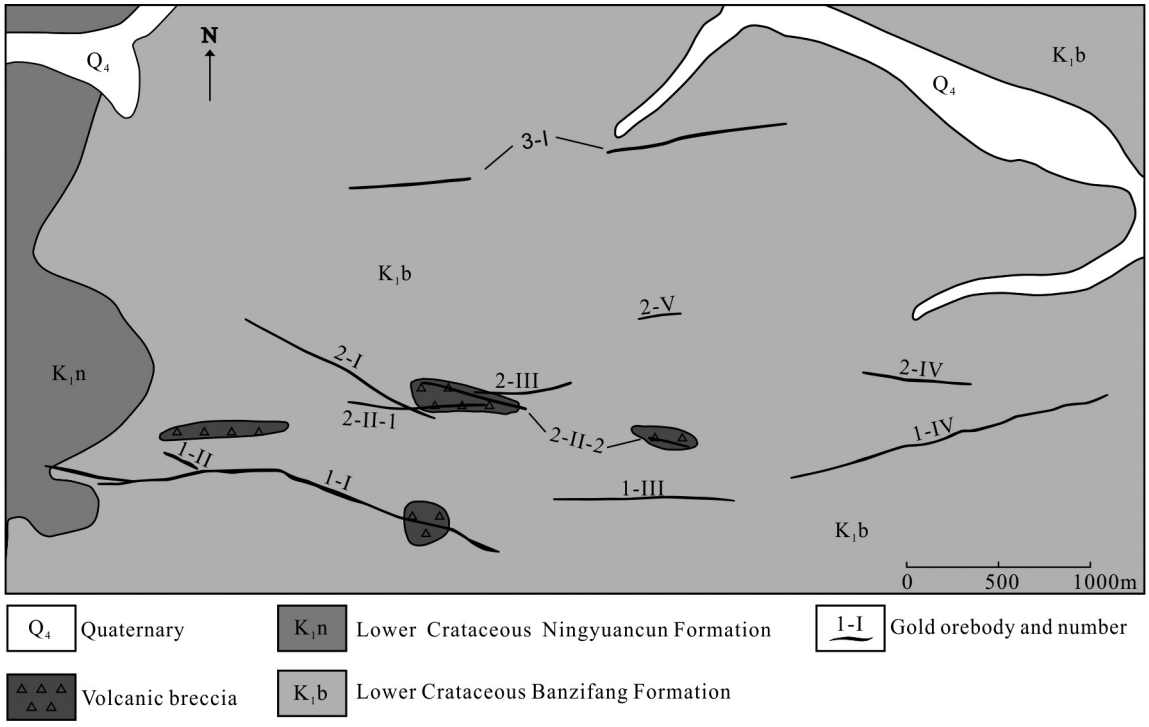

Figure 2. Geological sketch map of the Gaosongshan gold deposit (cited from Zheng, 2013).

Orebodies

Four auriferous quartz veins have been found in Gaosongshan gold deposit, which are subdivided into 11 mineralized zones or orebodies, trending NEE, NWW and approximately EW. Gold orebodies discovered in the Gaosongshan gold deposit are all situated in tectonoclastic zones and mainly occur as vein type bodies (Fig. 2), and their wall rocks primarily consist of andesite, volcanic breccia, tuff, and basalt. Among all the gold ore bodies, 1-I, 2-I and 2-II are NWW-trending to NW-trending; 1-II, 1-III, 2-II-1, 2-III, and 2-IV are close to EW-trending; and 1-IV, 3-I, and 3-II are NEE-trending. The 1-I gold ore body, the biggest one, is ~2 km long. It is controlled by different sets of fractures in different directions that the west part of this body is EW-trending and the east part is NWW-trending to SEE-trending (Fig. 2). It strikes ~56-368m long with the strike direction of 86-115° and the dip angle 55°-72°. The largest thickness is 7.90m, while the average thickness is 1.72m. The average grade of Au is 5.47g/t. The content of Au in this ore body accounts for 76.8% of the total resources in this mining area. Total measured, indicated, and inferred resources for the Gaosongshan gold deposit are 21.7tonnes of gold with the grade of 6.3g/t Au, making it one of the largest epithermal gold deposits in China.

Ore

Ores are generally divided into breccia type, quartz-vein type and altered rock type (Fig. 3a, b, c). For the first type, the breccia fragments are composed of poorly sorted angular clasts of altered andesite, volcanic breccia and tectonic breccia, which were cemented by quartz-sulfide veins and the breccia partly contains chlorite and illite alteration minerals and pyrite (Fig. 3a, g). Commonly, anhedral granular pyrite and lesser amount of chalcopyrite are presented in this siliceous cement (Fig. 3f). After oxidation and leaching, pyrite were oxidized into limonite, which occurs as veinlets or stockworks, meanwhile, part of the pyrites, are distributed as sparse disseminations or cloddy. Quartz-vein type can occur in many kinds of volcanic rocks, mainly andesite and volcanic breccia. These rocks were crosscut by quartz-sulfide vein, with pyrite occurring as fine-grained. Native gold, distributed in quartz vein, can also be observed in this ore type (Fig. 3b) and gold mineralization mainly occurs with silicification and pyritization. Altered rock type is strongly associated with intense silicification, pyritization, chloritization and illitization and its protolith are commonly volcanic breccia and tuff (Fig. 3c). Pyrite occurs as massive, dense disseminated in the gray quartz vein together with chlorite (Fig. 3d).

Mineralogy

Pyrite with minor chalcopyrite and native gold are present in the ores. Most of ore minerals are predominantly subhedral grains, although some displays euhedral, cubic or anhedral textures (Fig. 3c, f). Quartz, chlorite, illite, adularia, sericite, calcite, fluorite are gangue minerals and commonly occur as fine-grained assemblages, although some are medium- and micrograined assemblages. The ore minerals are distributed as sparse disseminated, locally as dense disseminated or scattered (Fig. 3c, e). Conversely, the gangue minerals occur as massive, veinlets or drusy structures (Fig. 3b, Fig. 4a, d). Sulfides are the major ore minerals, which generally account for less than 1vol. %. Pyrite is the most abundant sulfide coexisting with minor anhedral chalcopyrite, galena and sphalerite (Fig. 3f). Quartz is believed to be the most extensive gangue minerals in ores, accounting for more than 60% of the ores by volume. It occurs predominately as veinlets with sulfides or as stockworks individually. Gold grains occur as irregular, sheet or filiform and range in size from 0.1 to 10mm in diameter (Hao et al., 2014). They are distributed predominately along quartz crystal boundaries in the form of native gold. Secondly, lesser amounts of gold are enclosed in pyrite, in the form of native gold in the early stage and invisible cationic gold in the late stage, respectively. Adularia can be occasionally seen under the microscope with its typical rhombic section and is commonly closely associated with quartz and sericite (Fig. 3h). Adularia forms euhedral-subhedral platy and rhombic crystals with a diameter of <0.1mm. Calcite is a common mineral, developed as veins with quartz and chlorite (Fig. 3i, Fig. 4i). Fluorite is purple in color associated with quartz and chlorite and it occurs as anhedral assemblages (Fig. 4f).

Alteration

According to previous works (Zheng et al., 2015) and our field observations, the wall rock alteration minerals in the Gaosongshan gold deposit comprise quartz, adularia, chlorite, sericite, illite, fluorite, calcite and lesser amounts of pyrite. The quartz, adularia and pyrite alteration is spatially closely associated with gold mineralization. This hydrothermal alteration is mainly developed along faults and in volcanic rocks and breccia (Fig. 4a, b, c and e), showing an alteration zone, from the proximal mines with silicification, pyritization and adularization to the distal mines with sericitization, illitization and propylitization.

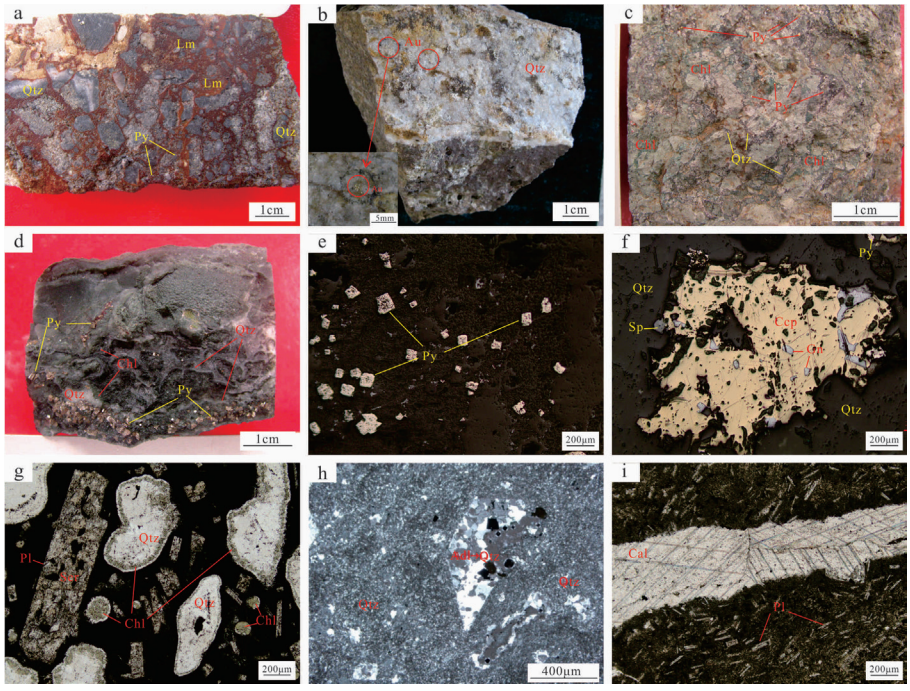

Figure 3. Photographs of representative hand specimens showing the types of gold ores (a, b, c) and microphotographs showing some ore minerals and gangue minerals in the Gaosongshan gold deposit. (a) breccia type: strongly altered volcanic breccia cemented by gray quartz-sulfide stockworks, most of the pyrite were oxidized into limonite; (b) quartz-vein type: breccia fragments were cemented by wide milky quartz with native gold; (c) altered rock type: volcanic breccia with intense silicification, pyritization, chloritization, pyrite sparsely disseminated in the gray quartz vein together with chlorite; (d) breccia fragments were cemented by quartz-pyrite-chlorite veins, with pyrite being cubic or subhedral-anhedral granular; (e) cubic pyrite disseminated in tectonic breccia; (f) anhedral chalcopyrite in quartz vein; (g) plagioclase in andesite altered into sericite, thin chlorite vein grow with quartz edge in amydaloidal structure; (h) adularia can be seen under the microscope with its typical rhombic section, part of adularia were replaced by quartz; (i) calcite vein with its typical rhombic cleavage. Photographs c and f were taken under reflected plane-polarized light, while figures g, h and i were taken under reflected crossed-polarized light. Qtz-quartz, Lm-limonite, Py-pyrite, Ccp-chalcopyrite, Chl-chlorite, Adl-adularia, Pl-plagioclase, Au-native gold, Ser-sericite, Cal-calcite

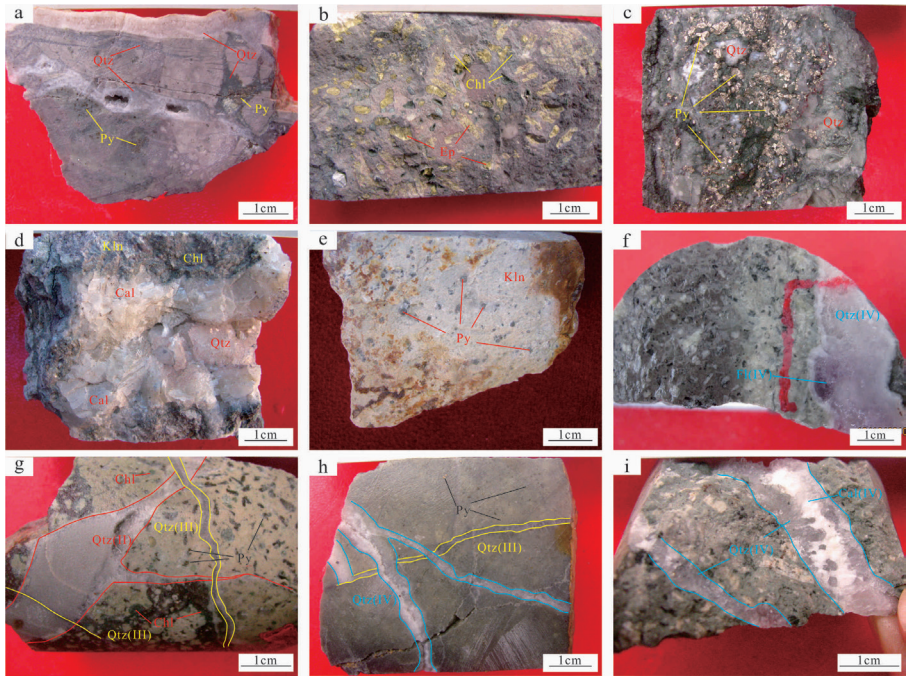

Figure 4. Photographs of mineralization and alteration styles. (a) extensive gray quartz veinlets, stockworks and milky quartz vein with drusy quartz developed in tectonic breccia with disseminated and massive pyrite; (b) purple volcanic breccia with strong chloritization and epidotization; (c) quartz-pyrite vein: cubic and euhedral-subhedral pyrite being massive distributed in milky quartz; (d) andesite with strong and extensive kaolinization and chloritization crosscut by 3cm quartz-calcite vein; (e) strongly kaolinization with some fine grained pyrite; (f) pruple-colored fluorite associated with white quartz (IV); (g) second-stage quartz vein cut by two third-stage quartz vein developed in silicified volcanic breccia with scattered xenomorphic granular pyrite; (h) second-stage quartz veinlet crosscut by fourth-stage quartz vein; (i) fourth-stage quartz-calcite vein, white calcite overgrows within quartz. Qtz-quartz, Py-pyrite, Chl-chlorite, Ep-epidote, Kln-kaolinite, Cal-calcite, Fl-fluorite

Based on ore textures, crosscutting relationships, and mineral assemblages, the hydrothermal mineralization process can be divided into four stages: chlorite/ epidote + pyrite + sericite + illite + adularia (stage I), quartz + pyrite (stage II), quartz + pyrite + Au (stage III), and quartz + carbonate + fluorite (stage IV). The quartz in stage II occur commonly as milky white stock-work vein or gray microcrystal veins (Fig. 4g). Stage III is considered to be the main stage for ore formation and is characterized by the occurrence of Au. Pyrite is scattered or disseminated in thin smoky gray quartz veins (Fig. 4h). The quartz in stage IV is characterized by milky veins or miarolitic cavities, associated with white calcite and purple fluorite (Fig. 4d, i). All above suggests that the Gaosongshan gold deposit is a typical low-sulfidation epithermal gold deposit (Zheng et al., 2014; Hao et al., 2016).

Sampling and analytical methods

Samples including quartz of stage II to stage IV, pyrites of stage II and III (Fig. 4), were collected from different ore bodies. In the preparation of samples, quartz and pyrite-bearing samples were crushed into a grain size of approximately 300 to 500μm using a pre-cleaned griddle and pestle. About 2g pure quartz grains and 1g pure pyrite grains were hand-picked using a binocular microscope to eliminate visible impurities. The calcite impurities on the surface were readily removed after 24hours of 10% HCl etching. Then all samples were washed with ultrapure water and then finally dried.

The thermoelectricity of pyrites was measured by BHTE-08 thermoelectric coefficient instrument (made by Beijing University of Aeronautics and Astronautics) at the Laboratory of Genetic Mineralogy, China University of Geosciences (Beijing). Parameters of this measuring instrument are as follows: reading accuracy is 0.1μV/°C, and its measuring accuracy is beyond 1%FS. Activation temperature was picked at 60°C with indication error small than 1°C. Each sample was randomly prepared 50 granules for testing.

100mg of each sample used in trace elements analysis were crushed again to a grain size of approximately less than 70μm using a carefully pre-cleaned agate mortar and pestle. Tests on the mortar and the pestle showed that contamination introduced in this way could be neglected. The analyses were carried out at the Ore Deposit Geochemistry Microanalysis Room, the State Key Laboratory of Geological Processes and Mineral Resources, China University of Geosciences (Beijing). 50±0.3 mg of powdered sample was weighed into a Teflon digestion vial, and 1 ml of HCl, 1 ml of HNO_3, 3 ml of HF, and less than 0.5 ml of concentrated $HClO_4$ were added. Screw the cap tightly and then it was heated for 48 hours at temperature 170°C on a hot plate. Unscrew the cap and until it was evaporated to saltlike residue. Then the residue was added with 2.5 ml HNO_3 and 2.5 ml ultrapure water. Screw the cap tightly and then it was heated for 12 hours at temperature 170°C on a hot plate. After cooling, the solution in the each vial was subsequently transferred into Teflon plastic bottles and made up with ultrapure water to a volume of 50 ml. ICP-MS analysis was carried out with Thermo Fisher X Series II Quadrupole Plasma Mass Spectrometer of America. The analytical accuracy is higher than 5% for element contents>10ppm, and higher than 10% for element contents<10ppm. In order to ensure data accuracy, standard samples, parallel samples and blank samples (2% HNO_3) were used during the experiment. 10ppb Rh solution was the internal standard for the ICP-MS measurements. Part of the analysis of pyrites was accomplished at Analytical Laboratory of Beijing Research Institute of Uranium Geology, and the ICP-MS instrument is a high resolution one (model Element I, Finnigan MAT). Experiments were conducted in accordance with general rules of DZ/T0223-2001 ICP-MS methods under the following conditions: temperature of 20°C, relative humidity of 30%.

Characteristics of Genetic Mineralogy of Pyrite and Quartz Thermoelectricity

Twenty-six pyrite samples, 1300 granules in total, were collected at different bodies in the Gaosongshan gold deposit, and the results are listed in Table 1. Based on pyroelectric coefficient, pyrite is divided into two types: (1) N-type ($\alpha < 0$ μV·℃$^{-1}$), and (2) P-type ($\alpha > 0$ μV·℃$^{-1}$). Conductive types of pyrites in this deposit belong to mixed type, with thermoelectric coefficients ranging from -262.6 μV·°C^{-1} to 335.6 μV·°C^{-1}. It can be concluded from Figure 5 that pyroelectric coefficient of N-type ranges from -262.6 μV·°C^{-1} to -1.6 μV·°C^{-1} with pronounced intervals at -161.7 μV·°C^{-1} to -15.1 μV·°C^{-1}. And those of P-type range from 1.6 μV·°C^{-1} to 335.6 μV·°C^{-1} with two respective pronounced intervals at 29.4-140.8 μV·°C^{-1} and 182.5 - 335.6 μV·°C^{-1}.

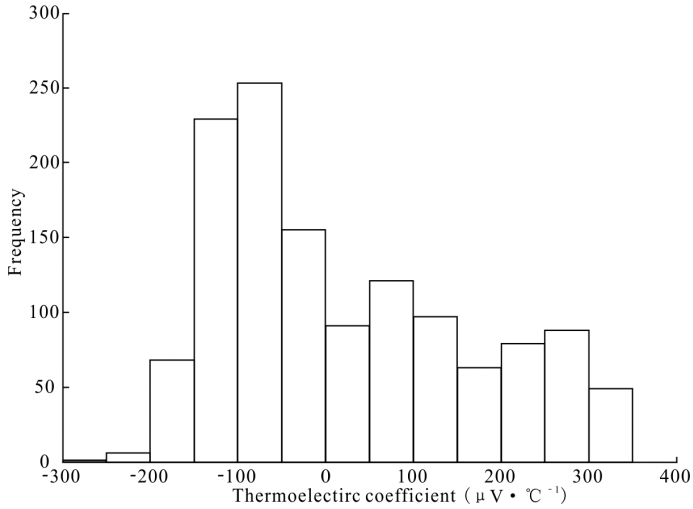

Figure 5. Frequency histogram of pyrites' thermoelectric coefficient

Rare earth elements

Pyrite

The measured REE concentrations of thirteen gold-bearing and nineteen Au-free pyrites in the Gaosongshan gold deposit are presented in Tables 2 and 3, and the chondrite-normalized curves are shown in Figure 6.

The total REE concentrations in ore-bearing pyrites are in the range of 9.75-139.43 ppm. The chondrite-normalized REE patterns are characterized by LREE enrichment. ΣLREE are 9.09-124.48 ppm, and ΣHREE are 0.6714.95 ppm. The LREE/HREE ratios are 7.37-13.68 (mean= 10.39). (La/Sm) N are 0.71-16.75 (mean= 4.77), and (Gd/Yb) N are 2.19-12.75 (mean= 8.69). Two samples, 1-II ZK1502-06 and 1-IZK8001-11/12, have positive Eu anomalies and the rest have obvious or weak negative Eu anomalies. Generally, δEu= 0.65-1.66 (mean= 0.93). δCe are 0.98-1.11, and the average value is 1.02, for which no Ce anomaly is observed.

The chondrite-normalized REE patterns for Au-free pyrites are similar to those of gold-bearing pyrites. ΣREE ranges from 4.75-123.91 ppm, ΣLREE are 4.07-115.47 ppm, ΣHREE are 0.69-9.16 ppm, and the ΣLREE/ΣHREE ratios are 5.9313.77 (average: 8.85). $(La/Sm)_N$ are 2.25-9.92 (mean= 4.77) and $(Gd/Yb)_N$ are 1.67-11.16 (mean= 5.42). Unlike the gold-bearing pyrites, Au-free pyrites display an obvious negative Eu anomaly and no Ce anomaly with δEu= 0.55-1.11 (mean= 0.82) and δCe = 0.92-1.10 (mean= 1.00).

Quartz

The REE concentrations and related parameters of quartz are given in Table 4 and the chondrite-normalized REE patterns are shown in Figure 7.

REE concentrations in ore-bearing quartz are lower than those in ore-bearing pyrites, ranging from 3.56 ppm to 10.08 ppm and those in barren quartz ranging from 0.47 ppm to 6.50 ppm, which are much smaller. The LREE and HREE contents in ore-bearing quartz are 3.27-9.37 ppm and 0.291.32 ppm, respectively, while those in barren quartz are 0.41-6.17 ppm and 0.060.33 ppm, respectively. The LREE/HREE ratios of ore-bearing quartz and barren quartz are 4.74-15.37 and 5.62-18.85, respectively. $(La/Yb)_N$ ratios of ore-bearing quartz and barren quartz are 7.59-50.22 and 5.36-75.53, respectively. The LREE enrichment chondrite-normalized REE patterns are characteristic of quartz in the Gaosongshan gold deposit (Fig.

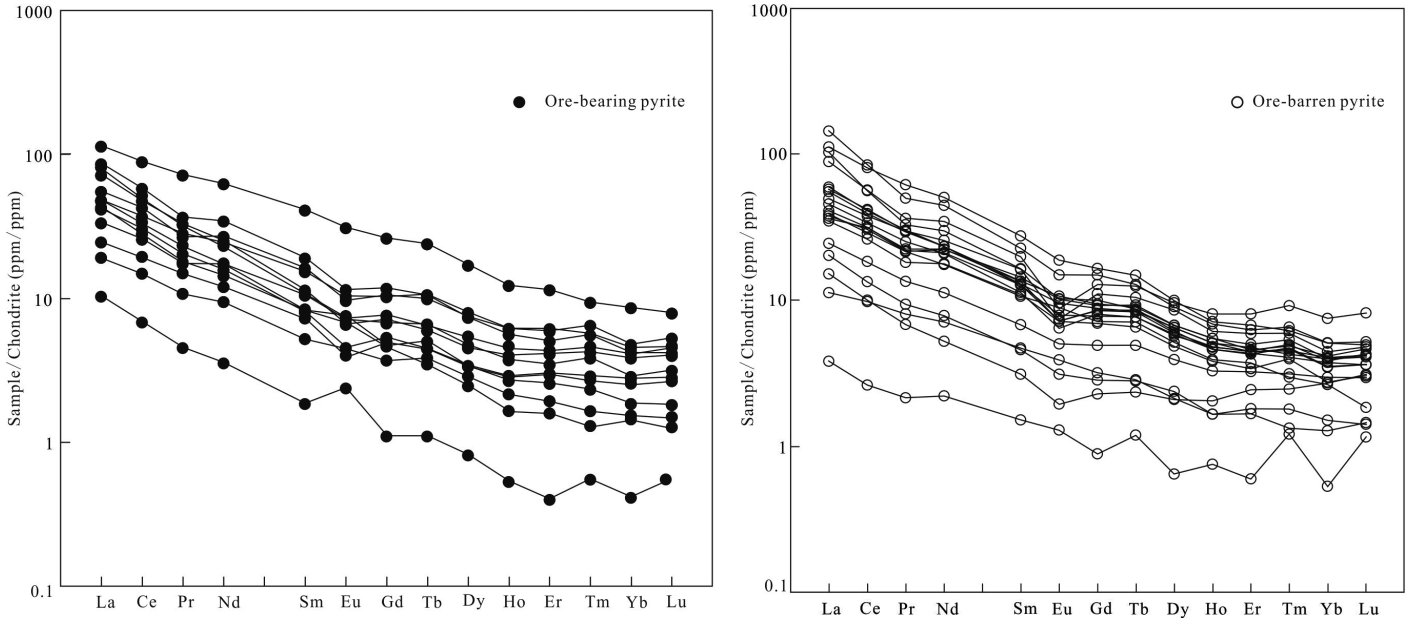

Figure 6. Chondrite-normalized REE patterns of pyrites from the Gaosongshan gold deposit. The chondrite values for the figures in this paper are from Sun and McDonough (1989).

7). The $(La/Sm)_N$ ratios and $(Gd/Yb)_N$ ratios for ore-bearing quartz are 2.85-7.41 and 2.19-5.97, respectively. Those for barren quartz are 3.06-13.29 and 1.1210.13. All the quartz samples are characterized by no Ce anomalies. δCe values range from 0.88 to 1.00 (average 0.96) in ore-bearing quartz and those range from 0.84 to 1.07, with an average of 0.96 in barren quartz. Barren quartz is characterized with obvious negative Eu anomalies (δEu = 0.45-0.95, average: 0.80). Meanwhile, the values of δEu are 0.66-1.62 (average: 1.03) in ore-bearing quartz in general, showing obvious negative Eu anomalies in samples 1-II ZK1502-07 and 2-II ZK9601-04\05, no Eu anomalies in samples 1-I ZK8001-05 and 1-I ZK9604-12, while sample 2-II ZK8004-03-2 exhibits a positive Eu anomaly.

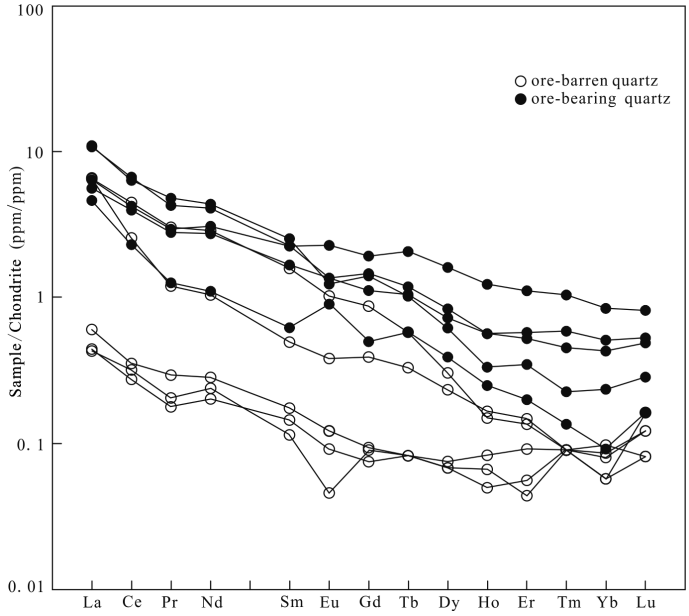

Figure 7. Rare earth element chondrite-normalized patterns of quartz from the Gaosongshan gold deposit.

Trace elements

The trace elements contents of thirteen ore-bearing pyrites in the Gaosongshan gold deposit are listed in Table 5, and those of the eighteen Au-free pyrites are listed in Table 6. A spider diagram of the portions of rare earth elements, lithophile elements, and high-field-strength elements with respect to the Chinese continental crust trace elements is shown in Figure 8.

Pyrite commonly contains a high level of trace elements, either hosted by substitution within the crystal lattice, such as Co and Ni replace Fe, and As, Se, and Te replace S, or as nanoparticles or micro-inclusions, such as Au, Ag, Cu, Pb, Zn, Sb, Bi, and W. Co and Ni are the common and abundant trace elements in pyrite, with Co contents of ore-bearing pyrites ranging from 51.3264.0ppm, with an average of 157.1ppm and Ni contents ranging from 68.9258.0ppm, with an average of 225.7ppm. The ratios of Co/Ni are 0.311.90, with an average of 0.92. The contents of Co in Au-free pyrites are 63.4426.0ppm, with an average of 170.6ppm. The contents of Ni are 16.0421.7ppm, with an average value of 126.9ppm. The ratios of Co/Ni are 0.335.36, with a mean value of 2.26. The ratios of Sr/Ba in ore-bearing pyrites are 0.110.50, with an average value of 0.24, and that of Au-free pyrites are 0.091.11, with an average value of 0.39.

The Hf/Sm ratios in ore-bearing pyrites are 0.28-0.94. The Nb/La and Th/La ratios are 0.06-0.28 and 0.05-0.22, respectively. The Y/Ho ratios are 23.80-27.28, except for that of one sample (1-IZK8001-11/12), the Zr/Hf ratios are 35.4147.83, and the Nb/Ta ratios are 10.96-18.52. The ratios of Hf/Sm, Nb/La, Th/La, Y/Ho, Zr/Hf, and Nb/Ta in ore-free pyrite are 0.39-1.17, 0.07-0.45, 0.06-0.28, 23.51-28.42, 33.99-48.87, and 12.61-22.84, respectively.

Ore-bearing pyrites and ore-free pyrites in the spider diagram of the trace elements generally exhibit similar characteristics, compared with the Chinese continental crust (Fig. 8). Pyrites consist of enriched Co, Ni, Cu, Zn, Pb, with enrichment coefficients higher than 2 and also comprise strongly depleted elements with enrichment coefficients less than 1, including Sr, Ba, Rb, and other large-ion lithophile elements, as well as high-field-strength elements (HFSE) such as Nb, Ta, Zr and Hf.

Discussion

The origin of pyrite

Trace element ratios, especially those for Co and Ni in pyrite appear to have been used to distinguish magmatic, hydrothermal and sedimentary origins of pyrites in ore deposition (Loftus-Hills and Solomon, 1967; Bralia et al., 1979; Bajwah et al., 1987; Brill, 1989). The Co/Ni ratio for magmatic pyrites is greater than 5 in most cases, and mostly greater than 10 (Bralia et al., 1979; Bajwah et al., 1987). The Co and Ni contents and the Co/Ni ratios in hydrothermal pyrites vary greatly; the Co and Ni contents can reach up to 1000ppm, and the Co/Ni ratios are generally greater than 1 and can show much variation. Sedimentary pyrites are generally characterized by low contents of Co and Ni and a Co/Ni ratio<1. Generally, Co contents, which

Table 1. Thermoelectric parameters of pyrites in the Gaosongshan gold deposit

Sample number	Geology	Elevation (m)	P-type(μV·°C^{-1})		N-type(μV·°C^{-1})		Frequency of P-type (%)	Gold grade(μg/g)
			α	Average	α	Average		
2-IIZK7201-1	Volcanic breccia	401.614	11.6~215.5	114.8	-123.1~-1.7	-56.9	48	-
2-IIZK7201-14	Andesite	300.10	1.7~237.9	88.7	-131.4~-10.1	-61.5	50	<0.1
2-IIZK9603-19	Tuff	108.179	-	-	-231.4~-10	-122.7	0	0.2
2-IIZK9603-20	Tuff	107.229	-	-	-143.3~-36.5	-102.6	0	<0.1
2-IIZK10401-20	Andesite	303.19	-	-	-206.4~-54.7	-136.9	0	0.31
2-IIZK10401-39	Andesite	297.891	-	-	-262.6~-18.5	-129.9	0	<0.1
2-IIZK19201-08	Volcanic breccia, ore body	307.07	6.6~61.8	32.6	-170.3~-1.7	-73.9	10	10.9
2-IIZK19203-B12	Tuff	217.38	-	-	-200.7~-25.1	-131.4	0	<0.1
3-IIZK11101-14	Volcanic breccia	262.54	52.0~213.6	133.5	-160~-18.3	-76.9	18	<0.1
2-IVFQ2-17	Volcanic breccia	-	240.8~335.6	313.0	-	—	100	-
2-IVFQ2-19	Volcanic breccia	-	6.8~302.2	111.7	-186.7~-5.1	-88.2	60	-
2-IVFQ2-23	Volcanic breccia	-	66.9~335.0	210.8	-95.2~-11.7	-42.1	92	-
2-IVFQ2-25	Tuff	-	31.5~289.3	148.9	-86.1~-28.6	-51.7	84	-
2-IIzk20001-14	Tuff, ore body	281.33	1.7~100.3	50.5	-13.4~-135.2	-59.7	16	-
2-IIzk20001-18	Volcanic breccia	276.43	5.0~197.7	58.1	-6.7~-138.8	-78.0	20	-
2-IIzk20001-25	Volcanic breccia	217.93	10.1~275.5	64.8	-25.1~-153.5	-82.7	32	-
2-IIzk20001-27	Volcanic breccia	203.03	18.4~88.5	53.1	-10~-148.3	-90.8	10	-
2-IZK4801-06-08	Andesite, ore body	-	5.0~207.2	72.0	-205.6~-16.3	-110.1	14	3.59
1-IVTK1-1	Andesite	360	226.8~296.1	259.7	-	-	100	-
1-IZK0001-09.10	Andesite	322.225	1.6~98.0	43.5	-117.4~-4.8	-61.1	14	0.7
1-IIZK1502-06	Andesite, ore body	282.47	43.6~234.0	121.8	-58.2~-11.6	-34.9	96	14.78
1-IZK2302-20	Tectonic breccia, ore body	204.75	1.6~314.0	116.2	-118.9~-1.6	-60.3	96	2.15
1-IZK2402-05	Volcanic breccia, mineralized body	119.58	117.7~318.7	242.6	-	-	100	0.59
1-IZK3902-15	Volcanic breccia	-	8.2~182.6	69.2	-150.7~-4.8	-45.3	64	0.32
1-IZK4701-20.28	Tectonic breccia	122.03	0~167.2	65.2	-162.4~-3.2	-48.7	62	0.18
1-IZK4703-10	Tectonic breccia, ore body	179.65	15.9~313.0	138.7	-83.7~-14.4	-47.4	88	1.19

Note: α in the table represents the thermoelectric coefficient range of each sample; numbers after symbol"<"are detection limits; symbol"-"represents no data.

Table 2. Rare earth element concentrations (ppm) and related parameters of ore-bearing pyrites from the Gaosongshan gold deposit

Sample r number	2-IIZK20001-14	2-IIZK19201-8	1-II ZK1502-06	2-IIZK10801-16	1-IZK8001-11, 12	2-II ZK9602-13	2-IIZK7201-14	1-IZK3102-10	1-IZK2302-20	2-I ZK4801-06, 08	1-IZK4703-10	1-IZK3902-08	3-IIZK7901-16
La	12.98	7.87	10.10	26.80	2.43	4.52	20.21	9.80	16.90	11.30	11.00	5.60	18.20
Ce	25.80	15.63	17.00	54.00	4.16	9.06	35.19	18.40	28.80	22.50	19.50	11.30	29.00
Pr	2.51	1.64	1.69	6.77	0.43	1.02	3.44	1.91	3.09	2.65	2.09	1.35	2.90
Nd	12.49	8.01	6.65	28.90	1.65	4.39	15.91	7.31	11.60	11.30	7.72	5.38	10.20
Sm	2.46	1.59	1.25	6.23	0.28	0.80	2.89	1.22	1.73	2.32	1.21	1.05	1.57
Eu	0.56	0.41	0.44	1.78	0.14	0.26	0.66	0.26	0.38	0.60	0.38	0.22	0.41
Gd	2.14	1.37	0.96	5.33	0.23	0.76	2.39	1.09	1.45	2.09	0.90	0.97	1.51
Tb	0.37	0.24	0.19	0.89	0.04	0.14	0.39	0.17	0.22	0.39	0.12	0.16	0.23
Dy	1.88	1.20	0.85	4.28	0.21	0.73	1.85	0.86	1.14	2.01	0.60	0.81	1.30
Ho	0.34	0.21	0.15	0.69	0.03	0.12	0.31	0.16	0.23	0.35	0.09	0.15	0.24
Er	0.97	0.57	0.42	1.88	0.07	0.32	0.83	0.50	0.68	1.01	0.25	0.47	0.69
Tm	0.16	0.10	0.06	0.24	0.01	0.04	0.14	0.07	0.11	0.14	0.03	0.07	0.11
Yb	0.81	0.48	0.31	1.45	0.07	0.26	0.70	0.47	0.65	0.77	0.23	0.41	0.67
Lu	0.13	0.08	0.05	0.20	0.01	0.04	0.10	0.07	0.10	0.12	0.03	0.06	0.11
Y	8.71	5.17	3.75	17.90	0.71	3.21	7.50	4.42	5.67	8.81	2.36	4.17	6.38
ΣREE	63.60	39.41	40.12	139.43	9.75	22.46	85.03	42.29	67.07	57.54	44.14	27.99	67.14
LREE	56.79	35.16	37.13	124.48	9.09	20.05	78.30	38.90	62.50	50.67	41.90	24.90	62.28
HREE	6.80	4.25	2.99	14.95	0.67	2.41	6.73	3.39	4.57	6.88	2.24	3.10	4.86
LREE/ HREE	8.35	8.26	12.42	8.33	13.64	8.31	11.64	11.49	13.68	7.37	18.67	8.04	12.82
$(La/Sm)_N$	3.41	3.19	3.23	16.75	0.71	2.70	4.51	3.68	4.90	7.81	2.36	3.48	5.24
$(Gd/Yb)_N$	2.19	2.35	11.50	7.43	12.71	7.41	2.81	10.57	12.75	6.49	17.72	7.15	11.89
$(La/Yb)_N$	11.54	11.67	23.07	13.26	24.90	12.42	20.60	15.05	18.71	10.57	34.31	9.87	19.54
δEu	0.74	0.85	1.22	0.94	1.66	1.02	0.77	0.69	0.73	0.83	1.10	0.65	0.81
δCe	1.11	1.07	1.01	0.98	1.00	1.03	1.03	1.04	0.98	1.01	1.00	1.01	0.98
Grade(μg/g)	-	10.9	14.78	1.09	1.01	1.61	-	1.98	2.15	3.59	1.19	1.135	1.08

Notes: $\delta Eu=(Eu)_N/((Sm)_N\times(Gd)_N)^{1/2}$, $\delta Ce=(Ce)_N/((La)_N\times(Pr)_N)^{1/2}$; ΣLREE/ΣHREE=Σ (La-Sm)/ Σ (Gd-Lu); symbol"-"represents no data.

Table 3. Rare earth element concentrations (ppm) and related parameters of Au-free pyrites from the Gaosongshan gold deposit

Sample	2-IIZK10401-20	1-IIZK1501-07	1-IZK8801-02	1-IZK0001-09, 10	1-IVTK1-1	1-IVTK1-2	2-II ZK9601-04	2-IIZK19203-B12	2-IIZK20001-1	2-IVFQ2-25	2-IIZK20001-25	2-IIZK20001-27	2-IVFQ2-19	1-IZK3902-15	1-IZK3101-13	1-IZK2402-05	1-IZK4701-20, 28	2-IVFQ2-17	3-IIZK7901-08
La	8.95	2.67	13.60	9.22	13.10	14.10	4.81	21.03	8.24	34.07	24.39	8.60	9.68	10.80	11.70	26.5	3.59	0.91	5.81
Ce	18.71	6.00	25.60	17.60	24.00	25.10	8.20	34.80	16.03	51.52	34.36	19.19	19.36	20.70	23.10	49.4	6.14	1.61	11.30
Pr	2.05	0.77	2.83	2.04	2.79	2.87	0.89	3.46	1.73	4.74	3.12	2.13	2.08	2.39	2.83	5.86	0.65	0.20	1.28
Nd	10.37	3.32	10.90	8.21	10.90	10.90	3.67	16.16	8.31	20.81	13.96	10.45	9.90	9.75	12.00	23.6	2.45	1.04	5.27
Sm	2.20	0.72	1.95	1.63	2.07	1.98	0.70	3.04	1.67	3.47	2.51	2.05	1.95	1.73	2.49	4.22	0.48	0.23	1.04
Eu	0.59	0.23	0.42	0.52	0.62	0.56	0.18	0.51	0.42	0.87	0.59	0.42	0.46	0.37	0.43	1.09	0.11	0.08	0.29
Gd	1.90	0.66	1.76	1.47	1.94	1.81	0.59	2.64	1.43	3.06	2.06	1.75	1.60	1.65	2.28	3.4	0.47	0.18	1.01
Tb	0.35	0.11	0.32	0.27	0.34	0.31	0.11	0.47	0.25	0.48	0.33	0.31	0.29	0.29	0.39	0.555	0.09	0.04	0.18
Dy	1.72	0.54	1.65	1.31	1.71	1.65	0.61	2.44	1.23	2.29	1.57	1.52	1.46	1.49	2.18	2.53	0.53	0.16	1.00
Ho	0.31	0.09	0.29	0.22	0.31	0.29	0.09	0.46	0.22	0.39	0.26	0.27	0.27	0.26	0.35	0.404	0.12	0.04	0.19
Er	0.83	0.28	0.79	0.62	0.76	0.74	0.30	1.34	0.56	1.04	0.71	0.73	0.75	0.72	0.98	1.12	0.41	0.10	0.54
Tm	0.14	0.03	0.11	0.08	0.12	0.12	0.05	0.23	0.10	0.17	0.12	0.12	0.13	0.10	0.15	0.158	0.06	0.03	0.08
Yb	0.68	0.22	0.67	0.45	0.71	0.69	0.26	1.28	0.47	0.87	0.60	0.59	0.65	0.64	0.76	0.865	0.46	0.09	0.51
Lu	0.11	0.04	0.10	0.05	0.12	0.11	0.04	0.21	0.08	0.13	0.09	0.09	0.11	0.09	0.12	0.126	0.08	0.03	0.08
Y	7.30	2.48	7.28	5.53	8.36	7.69	2.45	11.70	5.18	9.33	6.55	6.59	6.35	7.04	9.86	11	3.21	0.71	4.57
ΣREE	48.90	15.67	60.99	43.68	59.48	61.22	20.48	88.05	40.74	123.91	84.66	48.23	48.67	50.99	59.76	119.83	15.63	4.75	28.57
LREE	42.88	13.70	55.30	39.22	53.48	55.51	18.45	78.99	36.40	115.47	78.93	42.84	43.42	45.74	52.55	110.67	13.42	4.07	24.99
HREE	6.02	1.96	5.69	4.46	6.01	5.71	2.03	9.05	4.34	8.43	5.73	5.39	5.25	5.24	7.21	9.16	2.22	0.69	3.58
LREE/HREE	7.13	6.98	9.71	8.79	8.91	9.72	9.10	8.72	8.39	13.70	13.77	7.94	8.27	8.73	7.29	12.08	6.06	5.93	6.98
$(La/Sm)_N$	2.62	2.25	6.28	4.97	6.68	6.30	2.25	4.46	3.18	6.34	6.26	2.70	3.21	5.84	8.20	9.92	2.58	2.52	4.09
$(Gd/Yb)_N$	2.31	6.10	8.81	7.90	8.01	8.81	8.20	1.71	2.53	2.91	2.84	2.44	2.03	7.83	6.41	11.16	5.20	1.67	6.11
$(La/Yb)_N$	9.48	8.79	14.47	14.66	13.29	14.68	13.42	11.79	12.63	28.10	29.19	10.42	10.62	12.14	11.10	21.98	5.57	7.19	8.25
δEu	0.88	1.01	0.69	1.02	0.94	0.90	0.86	0.55	0.82	0.81	0.80	0.68	0.79	0.68	0.55	0.88	0.73	1.11	0.87
δCe	1.07	1.03	1.01	0.99	0.97	0.97	0.97	1.00	1.04	0.99	0.97	1.10	1.06	1.00	0.98	0.97	0.99	0.92	1.02
Grade(μg/g)	0.31	0.57	<0.1	0.7	-	-	0.65	-		-	-	-	-	0.32	0.55	0.59	0.18	-	0.13

Note: $\delta Eu=(Eu)_N/((Sm)_N\times(Gd)_N)^{1/2}$, $\delta Ce=(Ce)_N/((La)_N\times(Pr)_N)^{1/2}$, ΣLREE/ΣHREE=Σ(La-Sm)/Σ(Gd-Lu). "-"means no value.

Table 4. Rare earth element concentrations (ppm) and related parameters of quartz from the Gaosongshan gold deposit

Sample	Ore body					Non-ore body				
	1-I ZK8001-05	1-IZK9604-12	1-II ZK1502-07	2-IIZK9601-04\05	2-IIZK8004-03-2	2-IIZK9603-05-1	2-II TC9601-11	1-ITC16-1	1-ITC56-1	FQ2-33
La	1.32	1.51	2.53	2.58	1.09	1.55	0.14	0.10	0.10	1.53
Ce	2.41	2.56	4.05	3.86	1.40	1.56	0.22	0.19	0.17	2.72
Pr	0.26	0.28	0.40	0.45	0.12	0.11	0.03	0.02	0.02	0.29
Nd	1.27	1.43	1.90	2.03	0.51	0.48	0.13	0.11	0.09	1.33
Sm	0.25	0.34	0.34	0.38	0.09	0.08	0.03	0.02	0.02	0.24
Eu	0.08	0.13	0.08	0.07	0.05	0.02	0.01	0.00	0.01	0.06
Gd	0.23	0.39	0.30	0.29	0.10	0.08	0.02	0.02	0.02	0.18
Tb	0.04	0.08	0.04	0.04	0.02	0.01	0.00	0.00	0.00	0.02
Dy	0.18	0.41	0.21	0.16	0.10	0.06	0.02	0.02	0.02	0.08
Ho	0.03	0.07	0.03	0.02	0.01	0.01	0.00	0.00	0.00	0.01
Er	0.09	0.18	0.09	0.06	0.03	0.02	0.01	0.02	0.01	0.02
Tm	0.01	0.03	0.01	0.01	0.00	0.00	0.00	0.00	0.00	0.00
Yb	0.09	0.14	0.07	0.04	0.02	0.02	0.01	0.01	0.01	0.01
Lu	0.01	0.02	0.01	0.01	0.00	0.00	0.00	0.00	0.00	0.00
ΣREE	6.29	7.57	10.08	9.98	3.56	4.01	0.62	0.53	0.47	6.50
ΣLREE	5.60	6.25	9.31	9.37	3.27	3.80	0.55	0.45	0.41	6.17
ΣHREE	0.69	1.32	0.77	0.61	0.29	0.21	0.07	0.08	0.06	0.33
ΣLREE/ΣHREE	8.10	4.74	12.13	15.37	11.17	18.50	8.15	5.62	6.76	18.85
$(La/Sm)_N$	3.35	2.85	4.76	4.34	7.41	13.29	3.45	3.75	3.06	4.11
$(Gd/Yb)_N$	2.19	2.28	3.39	5.97	5.44	4.01	1.64	1.12	1.31	10.13
$(La/Yb_)N$	10.97	7.59	24.99	46.53	50.22	67.47	10.52	5.36	7.73	75.53
δEu	1.00	1.10	0.75	0.66	1.62	0.87	0.95	0.45	0.88	0.87
δCe	1.00	0.97	0.98	0.88	0.96	0.91	0.84	1.07	0.98	1.01

Note: $\delta Eu=(Eu)_N/((Sm)_N\times(Gd)_N)^{½}$, $\delta Ce=(Ce)_N/((La)_N\times(Pr)_N)^{½}$, ΣLREE/ΣHREE=Σ(La-Sm)/ Σ(Gd-Lu). Chondrite normalized values cited from Sun and McDonough ,1989.

Table 5. Trace element abundances (ppm) and related parameters of ore-bearing pyrites from the Gaosongshan gold deposit

Sample number	2-II ZK20001-14	2-II ZK19201-8	1-II ZK1502-06	2-II ZK10801-16	1-I ZK8001-11/12	2-II ZK9602-13	2-II ZK7201-14	1-I ZK3102-10	1-I ZK2302-20	2-I ZK4801-06/08	1-I ZK4703-10	1-I ZK3902-08	3-II ZK7901-16	Chinese continental crust
Li	1.28	0.90	1.31	80.00	0.57	1.40	1.44	1.42	0.74	1.40	0.87	0.70	1.93	44
Sc	4.56	1.97	1.14	10.80	0.31	1.37	4.26	0.59	0.72	1.82	0.48	1.05	1.49	11
V	7.12	12.66	6.74	95.70	6.13	5.90	11.47	2.42	2.09	13.00	1.59	3.69	9.70	99
Cr	4.33	2.71	17.80	170.00	4.42	12.40	0.96	5.30	9.33	16.80	6.79	6.92	6.00	63
Co	159.2	137.6	247.0	51.3	140.0	220.0	158.0	102.0	145.0	264.0	184.0	152.0	82.2	32
Ni	101.0	135.3	258.0	167.0	249.0	116.0	144.9	98.6	152.0	423.0	709.0	312.0	68.9	57
Cu	204	61	92	929	389	186	181	181	118	131	231	79	298	38
Zn	22	16	37	99	94	104	12	96	105	80	247	61	421	86
Ga	0.78	0.51	0.97	19.10	0.53	1.20	1.10	0.98	1.03	1.08	0.83	0.72	1.41	20
Rb	7.95	3.34	6.45	142.00	2.85	5.51	5.43	2.81	2.31	3.92	4.72	1.40	5.92	150
Sr	4.89	1.60	4.67	156.00	1.89	3.79	8.68	7.73	3.4	8.62	4.06	4.82	6.98	690
Y	8.71	5.17	3.75	17.90	0.71	3.21	7.50	4.42	5.67	8.81	2.36	4.17	6.38	27
Nb	2.18	2.14	0.83	2.91	0.63	0.88	2.32	1.19	1.63	1.71	0.70	1.56	1.62	34
Ba	22.4	11.0	20.1	407.0	6.9	11.9	17.5	45.9	31.5	58.6	14.0	43.0	24.9	610
Ta	0.20	0.15	0.05	0.24	0.01	0.05	0.15	0.08	0.09	0.10	0.05	0.09	0.09	3.5
Pb	207	234	207	65	161	322	372	445	378	226	293	251	4315	15
Th	2.46	1.67	0.50	3.54	0.13	0.52	2.20	1.58	1.72	2.28	1.11	1.24	2.18	17
U	0.92	0.58	0.16	0.91	0.14	0.14	0.63	0.47	0.59	0.64	0.37	0.44	0.69	5.6
Zr	79.92	55.81	12.50	95.10	9.24	14.4	76.93	41.40	46.80	54.60	30.30	39.50	65.20	160
Hf	1.99	1.39	0.35	2.47	0.15	0.40	1.61	1.02	1.15	1.39	0.75	0.99	1.48	5.1
Co/Ni	1.58	1.02	0.96	0.31	0.56	1.90	1.09	1.03	0.95	0.62	0.26	0.49	1.19	0.56
Hf/Sm	0.81	0.87	0.28	0.40	0.53	0.51	0.56	0.84	0.67	0.60	0.62	0.94	0.94	0.70
Nb/La	0.17	0.27	0.08	0.11	0.26	0.19	0.12	0.12	0.10	0.15	0.06	0.28	0.09	0.81
Nb/Ta	10.96	14.19	18.09	12.23	57.55	17.56	15.61	14.88	18.52	18.00	15.17	17.14	18.00	9.71
Th/La	0.19	0.21	0.05	0.13	0.05	0.12	0.11	0.16	0.10	0.20	0.10	0.22	0.12	0.41
Y/Ho	25.26	24.60	24.83	25.98	23.80	26.31	23.88	27.28	25.20	25.39	26.82	27.26	26.36	28.12
Zr/Hf	40.12	40.17	35.41	38.50	62.01	35.73	47.83	40.59	40.70	39.28	40.29	39.86	44.05	31.37
Sr/Ba	0.22	0.15	0.23	0.38	0.28	0.32	0.50	0.17	0.11	0.15	0.29	0.11	0.28	1.13

Note: Element abundances of Chinese continental crust are from Li and Ni, 1990.

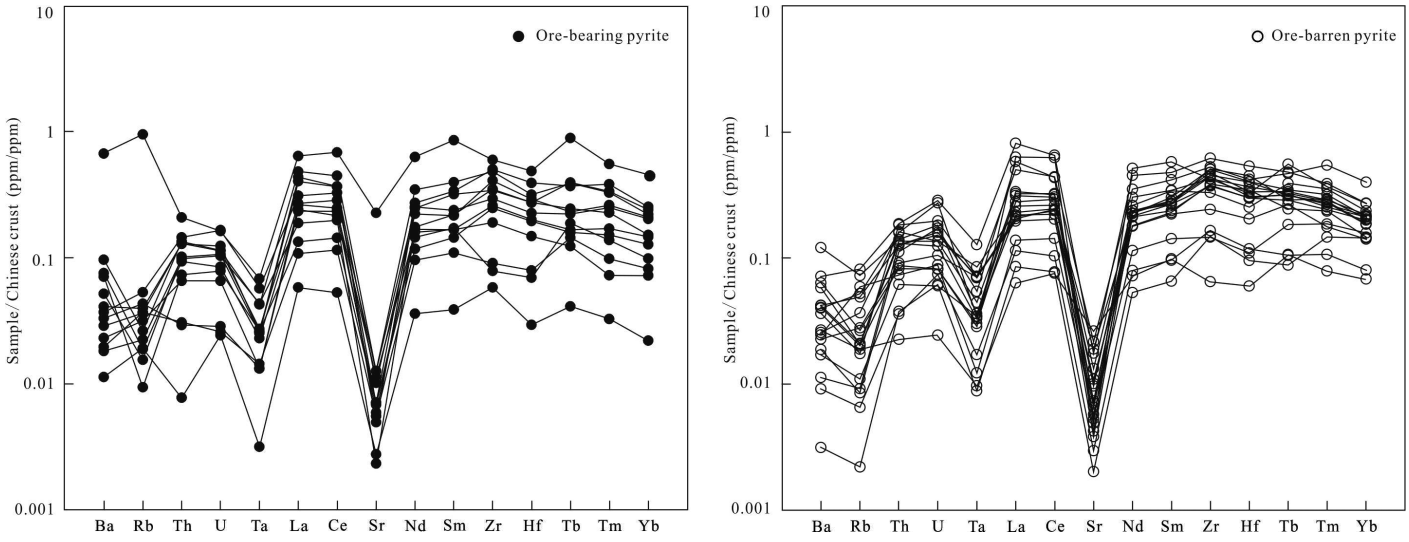

Figure 8. Spider diagram of trace elements of pyrites from the Gaosongshan gold deposit.

are less than 100ppm, are less than Ni contents (Chen et al., 1987). The Co and Ni contents of ore-bearing pyrites from the Gaosongshan gold deposit range from 51.3-264.0ppm and 68.9-258.0ppm, respectively. Average contents of Co and Ni are 157.1ppm and 225.7ppm, respectively. The Co/Ni ratios of ore-bearing pyrites are 0.31-1.90, with an average of 0.92. Ore-bearing and Au-free pyrites exhibit similar characteristics in the Co/Ni distribution diagram (Fig. 9). The Co contents hardly changes, while the Ni contents change considerably; the date points both cross the hydrothermal and sedimentary origin zones, while most data fall in the hydrothermal origin zone. Previous researches indicated that the Sr/Ba ratio in pyrite can be used as an indicator of the hydrothermal process and sedimentation (Ge and Han, 1987). A smaller ratio usually reflects a more explicit hydrothermal factor. The Sr/Ba ratios in ore-bearing pyrites from the Gaosongshan gold deposit range from 0.11 to 0.50, with an average of 0.24, while those in ore-free pyrites are 0.09-1.11, with an average of 0.39. In general, Co and Ni concentrations and Co/Ni ratio, the relatively small Sr/Ba ratio in pyrites, together with the obvious field characteristics of pyrites mentioned above, indicate that the pyrites are of hydrothermal origin.

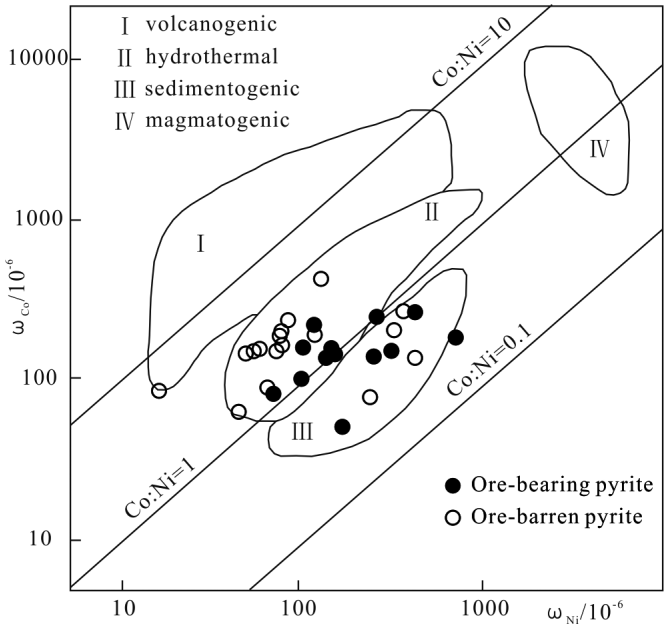

Figure 9. Co/Ni distribution diagram of pyrites from the Gaosongshan gold deposit. Boundaries of different geological settings are defined after Bajwah et al., 1987 and Brill, 1989.

Characteristics of ore-forming fluid

Minerals crystallizing in the same hydrothermal ore-forming evolutionary process have similar REE characteristics, which depend on the features and forming environments of the REE ore-forming fluids in the sedimentary process (Yuan et al., 1998). Lanthanide elements in quartz are prioritized to occurrence in fluid inclusions (Ghazi et al., 1993; Monecke et al., 2002; Götze, 2009). Meanwhile, the ionic radius of REE^{3+} and Fe^{2+} differ from each other, so it is difficult for REE^{3+} to replace the cations in the pyrite lattice; therefore, it is speculated that REEs in pyrite are mainly present in fluid inclusions. So REE characteristics of quartz reflect that of ore-forming fluid in equilibrium with quartz. Then REE compositions of pyrite coexist with quartz also show REE characteristic of ore-forming fluid. Therefore, REE characteristics of quartz and pyrite formed during main mineralization stage in the Gaosongshan gold deposit are representative of mineralization hydrothermal fluid REE compositions.

Figure 6 shows no distinctive differences in REE chondrite-normalized patterns of two types of pyrite, indicating that they may have the same origin. Similar results can be obtained from comparison between those of ore-bearing and barren quartz (Fig. 7). Pyrites and quartz show almost no Ce anomalies, no matter in ore-bearing samples or in ore-barren samples. However, obvious negative Eu anomalies are typical of ore-free pyrites (δEu= 0.55-1.11) and barren quartz (δEu= 0.45-0.95). Eu anomalies show a little complexity either in ore-bearing pyrites or in ore-bearing quartz. Except one sample shows a positive Eu anomaly (δEu= 1.62), the rest quartz samples show weak negative Eu anomalies. Similarly, with the exception of two ore-bearing pyrite samples showing positive Eu anomalies (δEu=1.22 and 1.66), the rest show significant or weak negative Eu anomalies. Eu anomalies in ore-bearing quartz and ore-bearing pyrites suggest that those anomalies partly reflect partitioning of Eu^{2+} into plagioclase during magmatic evolution. The two special pyrites and one quartz-sample showing positive anomalies were all sampled from altered andesite, in which contact with hydrothermal fluids, plagioclase alteration may release some Eu^{2+} into hydrothermal fluids causing Eu anomalies to be positive. The $(La/Yb)_N$ ratios of quartz show a negative correlation with formation depth of deposit (Zhao, 1997), indicating that the Gaosongshan gold deposit is a hypabyssal one, of which the $(La/Yb)_N$ is much higher than 1.

Wang et al. (2014) has analyzed the REE concentrations of ore-bearing volcanic rocks in the Lower Cretaceous Banzifang Formation, consisting of basaltic andesite, hornblende andesite, trachyandensite and andesitic volcanoclastic rock. ΣREE ranges from 114.46 to 166.16ppm with an average of 130.60ppm. $(La/Yb)_N$ are 5.41-7.11. δEu values are 0.86-1.07 with an average value of 0.94 and no obvious negative Eu anomalies. The chondrite-normalized REE patterns are characterized by LREE-enrichment. Despite somewhat variable REE concentrations, the shapes of the chondrite-normalized REE patterns of ore-bearing quartz, pyrites and volcanic rocks are quite similar with no obvious negative Eu anomalies,

Table 6. Trace element abundances (ppm) and related parameters of barren pyrites from the Gaosongshan gold deposit

Sample number	2-IIZK10401-20	1-IIZK1501-07	1-IZK8801-02	1-IZK0001-09, 10	1-IVTK 1-1	1-IVTK 1-2	2-II ZK9601-04	2-IIZK19203-B12	2-IIZK20001-1	2-IVFQ2-25	2-IIZK20001-25	2-IIZK20001-27	2-IVFQ2-19	1-IZK3902-15	1-IZK3101-13	1-IZK2402-05	1-IZK4701-20, 28	3-IIZK7901-08
Li	2.83	0.66	1.69	0.53	1.01	2.67	1.03	0.88	0.96	2.26	0.51	0.42	0.93	1.02	0.52	0.61	0.98	2.57
Sc	5.43	0.63	1.39	1.10	0.76	0.94	0.63	4.48	3.50	4.12	4.32	4.17	2.56	0.99	0.93	0.73	1.17	1.02
V	22.19	4.64	12.80	7.40	15.30	16.60	7.30	10.47	13.14	15.79	10.16	10.47	11.36	5.13	2.01	1.16	4.18	18.20
Cr	59.17	8.01	5.20	8.40	7.44	7.53	3.39	0.96	4.15	0.18	3.27	0.44	n. d.	8.46	5.89	4.73	6.61	14.70
Co	137.4	426.0	156.0	268.0	165.0	235.0	63.4	89.9	145.9	201.29	188.4	151.3	132.4	191.0	151.0	85.7	78.3	204.0
Ni	421.7	127.0	57.9	364.0	76.9	83.1	44.2	63.8	48.4	76.6	74.9	53.6	28.3	117.0	71.6	16.0	237.0	323.0
Cu	127	272	241	129	137	276	181	686	232	256	176	456	105	723	60	86	67	218
Zn	21	104	84	49	34	173	53	20	17	38	44	46	68	75	261	133	399	78
Ga	1.18	0.78	1.22	0.94	0.94	1.33	0.54	0.96	0.70	1.16	0.59	0.52	0.66	1.22	1.21	1.56	0.86	1.09
Rb	7.36	2.84	3.16	1.65	7.83	10.90	0.98	2.62	4.19	12.24	1.28	1.38	5.51	3.10	4.00	3.02	0.33	8.86
Sr	6.97	18.20	5.08	7.55	4.91	6.68	2.05	14.97	4.53	12.15	2.93	3.67	2.65	13.10	9.17	3.38	1.40	3.99
Y	7.30	2.48	7.28	5.53	8.36	7.69	2.45	11.70	5.18	9.33	6.55	6.60	6.35	7.04	9.86	11.00	3.21	4.57
Nb	3.3	0.7	2.3	2.3	1.8	2.9	1.5	3.4	3.1	5.7	3.1	3.3	4.4	1.7	2.1	1.9	0.4	0.6
Ba	25.7	16.4	25.6	10.4	24.4	73.6	5.6	22.1	13.9	43.6	11.5	6.9	15.7	35.4	38.8	24.8	1.9	15.0
Ta	0.24	0.03	0.16	0.12	0.12	0.13	0.06	0.25	0.25	0.45	0.19	0.25	0.30	0.12	0.11	0.10	0.03	0.04
Pb	242	292	832	167	436	616	212	241	201	539	277	222	497	308	203	455	86.	358
Th	2.15	0.39	2.31	1.05	2.70	2.38	0.61	3.11	1.55	3.18	1.90	2.16	2.75	2.22	1.40	1.48	0.64	1.25
U	0.90	0.14	0.76	0.34	1.53	1.02	0.42	1.10	0.59	1.60	0.97	0.85	0.76	0.70	0.46	0.46	0.35	0.49
Zr	80.71	10.40	59.50	38.90	76.10	70.50	26.40	84.42	61.62	98.98	67.95	72.42	81.19	60.40	52.90	67.60	23.80	23.40
Hf	2.06	0.31	1.53	1.04	1.71	1.56	0.60	2.14	1.77	2.73	1.87	2.04	2.29	1.52	1.29	1.66	0.49	0.56
Co/Ni	0.33	3.35	2.69	0.74	2.15	2.83	1.43	1.41	3.02	2.63	2.52	2.82	4.68	1.63	2.11	5.36	0.33	0.63
Hf/Sm	0.93	0.42	0.78	0.64	0.83	0.79	0.86	0.70	1.05	0.79	0.74	0.99	1.17	0.88	0.52	0.39	1.02	0.54
Nb/La	0.37	0.24	0.17	0.25	0.14	0.21	0.31	0.16	0.38	0.17	0.13	0.39	0.45	0.16	0.18	0.07	0.12	0.11
Nb/Ta	13.64	19.12	15.00	18.84	15.00	22.83	25.17	13.52	12.61	12.77	16.36	13.35	14.63	15.13	20.19	18.50	13.84	14.67
Th/La	0.24	0.14	0.17	0.11	0.21	0.17	0.13	0.15	0.19	0.09	0.08	0.25	0.28	0.21	0.12	0.06	0.18	0.22
Y/Ho	23.53	26.38	25.28	24.91	26.88	26.61	26.06	25.62	23.90	23.96	25.06	24.17	23.51	26.97	28.41	27.23	27.67	24.57
Zr/Hf	39.25	33.99	38.89	37.40	44.50	45.19	43.85	39.40	34.92	36.21	36.35	35.48	35.52	39.74	41.01	40.72	48.87	41.79
Sr/Ba	0.27	1.11	0.20	0.73	0.20	0.09	0.37	0.68	0.33	0.28	0.26	0.53	0.17	0.37	0.24	0.14	0.73	0.27

Note: n. d.-not detected.

which suggest that the partial melting processes played an important role in the rock formation and the plagioclase fractionation played a small role during magma evolution. It is likely that the ore-forming fluid was related to the andesitic magma.

The genetic relationship between different objects can be interpreted by using a correlating concentration of two trace elements to establish trace elements covariance diagram (Henderson, 1984). Geochemical parameters such as δEu and δCe can reflect the process of REE fractionation. This paper chose the δEu-δCe to plot the covariance diagram, which is obviously shown that the dot of ore-bearing quartz and pyrites are almost in the same region with volcanic rocks (Fig. 10), which indicates that ore-bearing quartz veins with pyrite have close relationship to volcanic rocks, reflecting that the ore-forming fluids are mainly from magmatic hydrothermal fluids. The stable isotopic compositions of oxygen and hydrogen studies of quartz in the Gaosongshan gold deposit find that $\delta^{18}O$=1.7 to 7.76‰, with an average of 3.5‰, while δD=–115 to –133 (Zheng et al., 2013); such data are different from both typical magmatic water and metamorphic water, but are much related to magmatic water and they are located in the right side of the meteoric water line, indicating that the ore-forming fluids originated from magmatic fluids mixed with atmospheric water.

Compared to Cl chondrite (Sun & McDonough, 1989), LREE is more enriched than HREE in pyrites; high field strength elements are strongly depleted; the Hf/Sm, Nb/La, and Th/La ratios are almost smaller than 1. Some trace element ratios in pyrites, such as Hf/Sm, Nb/La, Th/La, Y/Ho, Zr/Hf, Nb/Ta, have important significance in demonstrating the properties of ore-forming fluids (Oreskes and Einaudi, 1990; Yaxley et al., 1998). Recent studies showed that Cl-rich hydrothermal liquids are enriched in LREE, and the Hf/Sm, Nb/La, and Th/La ratios are less than 1 while the F-rich hydrothermal liquids are simultaneously enriched in LREE and HFSE with the Hf/Sm, Nb/La, and Th/La ratios generally larger than 1 (Oreskes and Einaudi, 1990; Bi et al., 2004; Mao et al., 2006). The quartz and pyrites are all enriched in LREE and the Hf/Sm, Nb/La, and Th/La ratios in pyrites are smaller than 1, indicating that the $C1^-$ contents in the ore-forming fluids of the Gaosongshan gold deposit may be slightly higher than the F^- contents, which was proven by the liquid-phase compositions analysis of the fluid inclusions in quartz (Liu, 2015).

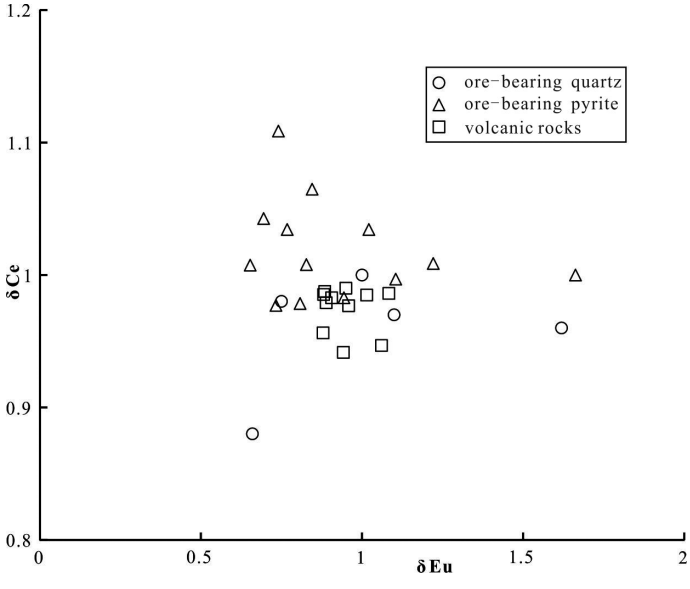

Figure 10. Bivariate scatter plot shows the relationship between δEu and δCe of ore-bearing quartz and pyrites and volcanic rocks from the Gaosongshan gold deposit. (Data points of volcanic rocks cited from Wang et al., 2014)

The REE contents of pyrite and the fractionation degree of LREE and HREE can be used to determine the depth of ore-forming fluids. In general, ore-forming fluids derived from mantle source materials are characterized by low REE content and slight differentiation of LREE and HREE (Zhao, 1997; Li et al., 2007). In this deposit, the differentiation of LREE and HREE in pyrite is large, with a relatively high REE content, which suggests that the ore-forming fluids are derived from crust source materials. Some trace elements in pyrite are similar to those in ore-bearing volcanic rocks, i.e., the Cr, Co, Ni, Cu and Zn contents are high (Wang et al., 2014), showing the extraction of some metal components from the surrounding rocks into the ore-forming fluids. Then, metallogenetic elements are released during fluid-wall rock interaction and join the mineralization processes. This conclusion is also consistent with the result indicated by S isotopes of pyrite that metal components originate from ore-bearing volcanic rocks (Zheng et al., 2013). Previous research on S isotopes in pyrites of this deposit show that the $\delta^{34}S$ values ranging from -4.3‰~2.8‰ with an average of -1.1‰ (Zheng et al., 2013). By combining the geological facts, i.e., that the sulfate minerals are not observed and the sulfides compositions are simplex in the deposit, it also can be stated that the pH and $f(O_2)$ of the fluid had no obvious change during the ore-forming process.

Y-Ho, Zr-Hf and Nb-Ta separately have the similar ionic radii and electrovalence, and thus, they often show the same geochemical characteristics, respectively. In many geological processes, Y/Ho, Zr/Hf, and Nb/Ta ratios are stable in one hydrothermal system; however, when the system is disturbed by hydrothermal activities or metasomatism, these element pairs will change significantly, and are presented as a large variation range among different samples (Bau et al., 1995; Yaxley et al., 1998). Y/Ho, Zr/Hf, and Nb/Ta ratios vary slightly (excluding one sample) in pyrites from the Gaosongshan gold deposit, showing that the hydrothermal system is relatively stable in the ore-forming process.

Application for prospecting

Analysis of thermoelectric properties of pyrites can provide information about depth of ore-forming, mineralization degree, and the medium conditions during the formation of deposits, and thus giving help on finding blind orebodies (Ji et al., 2013). Thermoelectric conductive type of pyrite has certain instructive significance to the erosion depth of the orebody. Based on the thermoelectric coefficient values, the thermoelectric parameters X_{NP} of pyrites are calculated by using the following equation (Xue et al., 2014), and can be qualitatively identify the denudation level of gold deposits.

$$X_{NP}= (2f_{I}+f_{II})-(f_{IV}+2f_{V}) \quad (1)$$

f_I represents the percentage of pyrite in the samples corresponding to the compensation pyroelectric coefficient: f_I means α>400μV·ºC -1; fII refers to α=200- 400μV·ºC^{-1}; f_{IV} refers to α=0 to -200μV·ºC^{-1}; and f_V means α < -200μV·ºC^{-1}. The X_{NP} value ranges from 200 to 100 for the uppermost orebody, 100-50 for the upper part of the orebody, 50 to -50 for the central orebody, and -50 to -100 for the lower orebody.

The X_{NP} values of different ore bodies in the Gaosongshan gold deposit are calculated: 1-I orebody, X_{NP}=-86 to 94, with an average of -10; 2-II orebody, X_{NP}=-106 to -46, with an average of -84.7; 2-IV orebody, X_{NP}=-32 to 50, with an average of 19. According to the above standard, the gold orebodies are eroded to their middle-lower part in different ore veins. The denudation percentage γ (γ=50-X_{NP}/4) of the orebody with respect to the total length of mineralization can be calculated using the thermoelectricity parameter: 1-I orebody, 26.5% to 71.5%; 2-II orebody, 61.5% to 76.5%; 2-IV orebody, 37.5% to 58%. These results are in accordance with those obtained by thermoelectric parameters X_{NP}.

Differences in the thermoelectric properties of pyrite essentially reflect physical and chemical changes during the migration of the ore-forming solution (Li et al., 2009; Zhai et al., 2013). According to the vertical zoning sequence of the primary halo in general hydrothermal deposits, halos of Co and Ni often exist in the lower part of the orebody while those

of S and As exist in the upper part. Co and Ni are present as isomorphism substituting for Fe^{2+}, resulting in N-type conductivity of pyrite. Meanwhile, replacement of S with As leads to P-type conductivity. In general, the zoning of thermoelectric conductivity in the vertical direction is as follows: upper part of the orebody, P-type; central part, P+N type, and lower part, N-type. From the relationship between the occurrence rate of the P-type pyrite and the elevation (Fig. 11), it is concluded that the P-type pyrite occurrence rate and elevation do not have a clear linear relation no matter what its wall rock is. Probably because the vertical spacing between sample collection points is no more than about 300 m, which is very small in the scope of ore formation. The non-linear relationship between the sample points may suggest that the pre-formed orebodies were superimposed and modified by the post-formed orebodies, resulting in pyrite with mixed thermoelectric conductivity at the identical depth. Researches on geochemistry of primary halo also indicate that in the longitudinal direction, the superimposition of ore-forming elements, the front halo elements, halo elements near the ore, and tail halo elements show superposition characteristics of multi-stage mineralization (Lian et al., 2010; Lv, 2012).

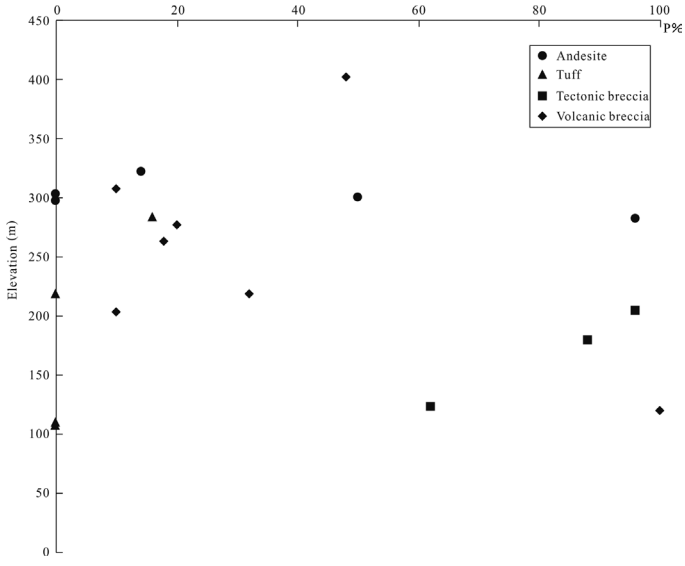

Figure 11. The relationship between the occurrence rate of P-type pyrites and its elevations

In summary, from 1-I orebody to 2-II body, the occurrence rate of P-type pyrite declines from 70.7% to 15.7%, that is to say, from the southwest to the northeast of this mining area, the denudation degree of orebody becomes increasingly strong. The electronic conductivity type of pyrite in orebody I is P-type to P-N type with fairly good ore-bearing potential. Those in orebody 2-II is transferred from the mix type to N-type from the west to the east direction, indicating that gold mineralization gradually weakens from west to east. The southeast part of this mining area may be more valuable for finding orebodies.

Conclusions

1. The chondrite-normalized REE patterns of pyrites and quartz are LREE-enriched. Barren quartz and pyrites are characterized by obvious negative Eu anomalies, while ore-bearing quartz and pyrite generally exhibit no Eu anomalies. Similar REE characteristics of ore-bearing quartz and pyrites and volcanic rocks, together with oxygen and hydrogen isotope studies of quartz, suggest that the ore-forming fluids of the Gaosongshan gold deposit were mainly magmatic origin which was associated with andesitic magma and was partly mixed with atmospheric water. Trace elements characteristics of ore-bearing pyrites and quartz, together with those of volcanic rocks indicate that the ore-forming materials were derived from the surrounding rocks.

2. Variable concentrations range of Co and Ni and Co/Ni ratio (0.31-1.90, average 0.92), together with relatively small Sr/Ba ratio in ore-bearing pyrites, support a hydrothermal origin of mineralization at Gaosongshan gold deposit. Slight changes of Y/Ho, Zr/Hf, Nb/Ta in ore-bearing pyrites indicate that the ore-forming hydrothermal solution has no obvious change in pH and *f* (O2) during the ore-forming process.

3. Pyrites are enriched in Co, Ni, Cu, Zn, Pb, with enrichment coefficients higher than 2. Large-ion lithophile elements (such as, Sr, Ba, Rb), as well as high-field-strength elements, such as Nb, Ta, Zr and Hf are strongly depleted with enrichment coefficients less than 1.

4. The electronic conductivity of pyrites in the Gaosongshan gold deposit is hybrid type. Thermoelectric parameters X_{NP} and denudation percentage γ of pyrites from orebodies 1-I, 2-II and 2-IV all indicate that the gold orebodies were eroded to their middle-lower part. From 1-I orebody in the southeast of the mining zone to 2-II orebody in the northwest, the P-type occurrence rate of the pyrite gradually decreases, suggesting that orebody erosion is increasingly intense. The southeast part of this mining area may be more valuable for finding orebodies.

Acknowledgements

This research was supported by Geological Survey Projects of China Geological Survey (grant no. 1212011120686). We thank our colleagues for their great support during the geological and deposit investigations at the Gaosongshan gold mine and for their assistance in genetic mineralogy analyses. We are grateful to the technicians, authors of exploration reports and previously published papers whose work contributed to this article.

References

Arribas, A. Jr. (1995). Characteristics of high-sulfidation epithermal deposits, and their relation to magmatic fluid. *Mineralogical Association of Canada Short Courses Notes,* 23, 419-454.

Bajwah, Z. U., Seccombe, P. K. & Offier, R. (1987). Trace element distribution, Co: Ni ratios and genesis of the Big Cadia iron-copper deposit, New South Wales, Australia. *Mineralium Deposita,* 22(4), 292-300.

Bau, M. & Dulski, P. (1995). Comparative study of yttrium and rare-earth element behaviours in fluorine-rich hydrothermal fluids. *Contributions to Mineralogy and Petrology*, 119(2-3), 213-223.

Bi, X. W., Hu, R. Z., Peng, J. T. & Wu, K. X. (2004). REE and HFSE geochemical characteristics of pyrites in Yao'an gold deposit: tracing ore forming fluid signatures (in Chinese with English abstract). *Bulletin of Mineralogy, Petrology and Geochemistry*, 23(1), 1-4.

Bie, F. L., Hou, Z. Q., Li, S. R., Su, W. C. & Xu, J. H. (2000). Composition characteristics of rare earth elements in metallogenetic fluid of the Gacun super large 'Kuroko'-type deposit (in Chinese with English abstract). *Acta Petrologica Sinica*, 16(4), 575-580.

Bonham, H. F. (1986). Models for volcanic-hosted epithermal precious metal deposits: a review. In: *International Volcanological Congress, Symposium 5*. Hamilton, New Zealand, 13-17.

Bralia, A., Sabatini, G. & Troja, F. (1979). A revaluation of the Co/Ni ratio in pyrite as geochemical tool in ore genesis problems: evidences from southern Tuscany pyritic deposits. *Mineralium Deposita*, 14(3), 353-374.

Brill, B. A. (1989). Trace element contents and partitioning of elements in ore minerals from the CSA Cu-Pb-Zn deposit, Australia. *Canadian Mineralogist*, 27(2), 263-274.

Chen, G. W., Xia, B., Xiao, Z. Y., Yu, H. X., Wang, H., Zhong, Z. H. & Wang, G. Q. (2001). Characteristics of epithermal deposits and the prospecting guide in China (in Chinese with English abstract). *Geology and Resources*, 10(3), 165-171.

Chen, G. Y. (1987). *Genetic mineralogy and prospecting mineralogy* (in Chinese). Chongqing Publishing House, Chongqing, 874pp.

Chen, Y. J., Pirajno, F., Wu, G., Qi, J. P. & Xiong, X. L. (2012). Epithermal deposits in north Xinjiang, NW China. *International Journal of Earth Sciences*, 101(4), 889-917.

Cooke, D. R., & Simmons, S. F. (2000). Characteristics and genesis of epithermal gold deposits. *Reviews in Economic Geology*, 13, 221-244.

Date, A. R. & Gray, A. L. (1985). Determination of trace elements in geological samples by inductively coupled plasma source mass spectrometry. *Spectrochimica Acta Part B: Atomic Spectroscopy,* 40(1), 115-122.

Dennen, W. H. (1967). Trace elements in quartz as indicators of provenance. *Geological Society of America Bulletin*, 78(1), 125-130.

Fan, J. G, Ni, P., Su, W. C., Qi, L. & Tian, J. H. (2000). Characteristics and significance of rare earth elements in quartz of Sidaogou hydrothermal gold deposit, Liaoning (in Chinese with English abstract). *Acta Petrologica Sinica,* 16(4), 587-590.

Franchini, M., McFarlane, C., Maydagán, L., Reich, M., Lentz, D.R., Meinert, L. & Bouhier, V. (2015). Trace metals in pyrite and marcasite from the Agua Rica porphyry-high sulfidation epithermal deposit, Catamarca, Argentina: Textural features and metal zoning at the porphyry to epithermal transition. *Ore Geology Reviews*, 66, 366-387.

Ge, C. H. & Han, F. (1987). *Geology and geochemistry of the exhalation sedimentary genesis ore deposit at Dabaoshan, Guangdong Province* (in Chinese). Science and Technology Publishing House, Beijing, 111pp.

Ghazi, A. M., Vanko, D. A., Roedder, E. & Seeley, R. C. (1993). Determination of rare earth elements in fluid inclusions by inductively coupled plasma-mass spectrometry (ICP-MS). *Geochimica et Cosmochimica Acta,* 57(18), 4513-4516.

Götze, J. (2009). Chemistry, textures and physical properties of quartz-geological interpretation and technical application. *Mineralogical Magazine*, 73(4), 645-671.

Hao, B. W., Deng, J., Bagas, L., Ge, L. S., Nie, F. J., Turner, S. & Qing, M. (2016) The Gaosongshan epithermal gold deposit in the Lesser Hinggan Range of the Heilongjiang Province, NE China: Implications for Early Cretaceous mineralization. *Ore Geology Reviews,* 73(2), 179-197.

Hao, B. W., Zhang, W. Z., Ge, L. S., Qing, M., Zhu, P., Zhao, H. H., Xue, J. G. & Ren, C. T. (2014). Study of gold enriched mechanism of Gaosongshan epithermal gold deposit in Lesser Xingan Range, NE of China (in Chinese with English abstract). *Journal of Mineralogy and Petrology,* 34(2), 48-59.

HBGMR (Heilongjiang Bureau of Geology and Mineral Resources). (1993). *Regional geology of Heilongjiang Province (in Chinese)*. Geological Publishing House, Beijing, 736pp.

Heald, P., Foley, N. K. & Hayba, D. O. (1987). Comparative anatomy of volcanic-hosted epithermal deposits: acid-sulfate and adularia-sericite types. *Economic Geology,* 82(1), 1-26.

Hedenquist, J. W. & Lowenstern, J. B. (1994) The role of magmas in the formation of hydrothermal ore deposits. *Nature,* 370(18), 519-527.

Hedenquist, J. W., Arribas, A. Jr. & Reynolds, T. J. (1998). Evolution of an intrusion-centered hydrothermal system: Far Southeast-Lepanto porphyry and epithermal Cu-Au deposits, Philippines. *Economic Geology,* 93(4), 373-404.

Hedenquist, J. W., Arribas, R. A. & Gonzalez-Urien, E. (2000). Exploration for epithermal gold deposits. *Reviews in Economic Geology*, 13, 245-277.

Henderson, P. (1984). *General geochemical properties and abundance of the rare earth elements.* In: Henderson, P. (Ed.), Developments in Geochemistry. Elsevier, Amsterdam, pp. 1-32.

Hill, P. A. & Green, R. (1962). Thermoelectricity and resistivity of pyrite from Renison Bell and Mount Bischoff, Tasmania. *Economic Geology*, 57(4), 579-586.

IMBGMR (Inner Mongolian Bureau of Geology and Mineral Resources). (1991). *Regional Geology of Inner Mongolian Automo* (in Chinese with English summary). Geological Publishing House, Beijing, 725pp.

Jiang, S. H., Nie, F. J., Zhang, Y. & Hu, P. (2004). The latest advances in the research of epithermal deposits (in Chinese with English abstract). *Earth Science Frontiers*, 11(2), 401-411.

Ji, X. Z., Yang, L. Q. & Wang, Z. L. (2013). Thermoelectricity characteristics of pyrite from Xincheng gold deposit, Eastern Shangdong (in Chinese with English abstract). *Geoscience,* 27(1), 37-45.

Kantipuly, C. J., & Westland, A. D. (1988). Review of methods for the determination of lanthanides in geological samples. *Talanta,* 35(1), 1-13.

Kerrich, R., Goldfarb, R., Groves, D., Garwin, S. & Jia, Y. F. (2000). The characteristics, origins, and geodynamic settings of supergiant gold metallogenic provinces. *Science in China Series D: Earth Sciences*, 43(1), 1-68.

Klinkhammer, G. P., Elderfield, H., Edmond, J. M. & Mitra, A. (1994). Geochemical implications of rare earth element patterns in hydrothermal fluids from mid-ocean ridges. *Geochimica et Cosmochimica Acta*, 58(23), 5105-5113.

Lian, Y. L., Hu, T. X., Shao, C. L., Yang, J. B. & Liang, C. L. (2010). Trace element geochemistry of the Gaosongshan gold deposit in Xunke County, Heilongjiang Province (in Chinese with English abstract). *Geology and Resources*, 19(4), 287-291.

Li, C. L., Li S. R., Luo, J. Y., Song, J. Y. & Zhang, J. Q. (2009). Thermoelectric coefficient, conductive type and significance of the pyrite from Yixingzhai Gold Deposit in Fanshi County, Shanxi Province, China (in Chinese with English abstract). *Geoscience,* 23(6), 1056-1063.

Lichte, F. E., Meier, A. L. & Crock, J.G. (1987). Determination of the rare-earth elements in geological materials by inductively coupled plasma mass spectrometry. *Analytical Chemistry*, 59(8), 1150-1157.

Li, H. M., Shen, Y. C., Mao, J. W., Liu, T. B. & Zhu, H. P. (2004). Features of trace elements in pyrite, quartz and their fluid inclusions: an example from Jiaojia-type gold deposits, northwestern Jiaodong peninsula (in Chinese with English abstract). *Chinese Journal of Geology*, 39(3), 320-328.

Li, H. M., Shen, Y. C., Mao, J. W., Liu, T. B. & Zhu, H. P. (2003). REE features of quartz and pyrite and their fluid inclusions: an example of Jiaojia-type gold deposits, northwestern Jiaodong peninsula (in Chinese with English abstract). *Acta Petrologica Sinica*, 19(2), 267-274.

Lindgren, W. (1933). *Mineral Deposits*. 4th ed. McGraw-Hill, New York, 930pp.

Li, T. & Ni, S. B. (1990). *Abundance of chemical elements in the earth and crust* (in Chinese). Geological Publishing House, Beijing, 136pp.

Li, Y. H., Yan, Y. F., Tan, J. & Li, F. (2007). The application of rare earth elements in research of ore deposits (in Chinese with English abstract). *Contributions to Geology and Mineral Resources Research*, 22(4), 294-298.

Li, S. R., Chen, G. Y., Shao, W. & Sun, D. S. (1996). *Genetic mineralogy of Rushan gold field, Jiaodong, China* (in Chinese). Geological Publishing House, Beijing, 116pp.

Liu, R. P. (2015). Magma, fluids and gold mineralization of the porphyry-epithermal gold deposits in the Yichun area, Heilongjiang Province (in Chinese with English abstract). Ph.D. Thesis, China University of Geosciences (Beijing), China.

Liu, X. S. (1995). Current status and prospect for the determination of rare earth elements by inductively coupled plasma mass spectrometry (in Chinese with English abstract). *Chinese Journal of Analytical Chemistry,* 23(10), 1218-1224.

Loftus-Hills, G. & Solomon, M. (1967). Cobalt, nickel and selenium in sulphides as indicators of ore genesis. *Mineralium Deposita*, 2(3), 228-242.

Lottermoser, B. G. (1992). Rare earth elements and hydrothermal ore formation processes. *Ore Geology Reviews*, 7(1), 25-41.

Lv, P. R. (2012). *Geochemistry of primary halos and evaluation of deep mineralization in the Gaosongshan gold deposit* (in Chinese). Master's Thesis, China University of Geosciences (Beijing), China.

Mao, G. Z., Hua, R. M., Gao, J. F., Zhao, K. D., Long, G. M., Lu, H. J. & Yao, J. M. (2006). REE composition and trace element features of gold-bearing pyrite in Jinshan gold deposit, Jiangxi Province (in Chinese with English abstract). *Mineral Deposits*, 25(4), 412-426.

Michard, A. & Albarède, F. (1986). The REE content of some hydrothermal fluids. *Chemical Geology*, 55(1), 51-60.

Monecke, T., Kempe, U. & Götze, J. (2002). Genetic significance of the trace element content in metamorphic and hydrothermal quartz: a reconnaissance study. *Earth and Planetary Science Letters*, 202(3), 709-724.

Oreskes, N. & Einaudi, M. T. (1990). Origin of rare earth element-enriched hematite breccias at the Olympic Dam Cu-U-Au-Ag Deposit, Roxby Downs, South Australia. *Economic Geology*, 85(1), 1-28.

Ouyang, H. G., Mao, J. W., Santosh, M., Zhou, J., Zhou, Z. H., Wu, Y. & Hou, L. (2013). Geodynamic setting of Mesozoic magmatism in NE China and surrounding regions: perspectives from spatio-temporal distribution patterns of ore deposits. *Journal of Asian Earth Science*, 78, 222-236.

Qi, J. P., Chen, Y. J. & Pirajno, F. (2005). Geological characteristics and tectonic setting of the epithermal deposits in northeast China (in Chinese with English abstract). *Journal of Mineralogy and Petrology,* 25(2), 47-59.

Sengör, A. M. C., Natal'in, B. A. & Burtman, V. S. (1993). Evolution of the Altaid tectonic collage and Palaeozoic crustal growth in Eurasia. *Nature,* 364(6435), 299-307.

Shao, J. L. (1988). *Gold Prospecting Mineralogy* (in Chinese). China University of Geosciences Press, Wuhan, 163pp.

Shao, W., Chen, G. Y. & Sun, D. S. (1990). Method of investigating thermoelectricity of pyrite and its application to pyrites from gold deposits in Jiaodong region (in Chinese with English abstract). *Geoscience,* 4(1), 46–57.

Sillitoe, R. H. (2008). Major gold deposits and belts of the North and South American Cordillera: distribution, tectonomagmatic settings, and metallogenic considerations. *Economic Geology,* 103(4), 663-687.

Su, W. C., Qi, L., Hu, R. Z. & Zhang, G. P. (1998). Determination of the rare earth elements in fluid inclusions by ICP-MS (in Chinese). *Chinese Science Bulletin*, 43(10), 1094-1098.

Sun, S. S. & McDonough, W. F. (1989). Chemical and isotopic systematics of oceanic basalts: implications for mantle composition and processes. *Geological Society, London, Special Publications,* 42(1), 313-345.

Wang, J. L., Gu, X. X., Zhang, Y. M., Liu, R. P. & Zheng, L. (2014). Petrogenesis and tectonic implications of volcanic rocks in the Gaosongshan gold deposit, Heilongjiang Province (in Chinese with English abstract). *Bulletin of Mineralogy, Petrology and Geochemistry,* 33(5), 561-571, 597.

Wang, Y. B., Zeng, Q. D., Zhou, L. L., Chu, S. X. & Guo, Y. P. (2016). The sources of ore-forming material in the low-sulfidation epithermal Wulaga gold deposit, NE China: Constraints from S, Pb isotopes and REE pattern. *Ore Geology Reviews*, 76, 140-151.

White, N. C. & Hedenquist, J. W. (1990). Epithermal environments and styles of mineralization: Variations and their causes, and guidelines for exploration. *Journal of Geochemical Exploration*, 36(1), 445-474.

White, N. C. & Hedenquist, J. W. (1995). Epithermal gold deposits: Styles, characteristics and exploration. *Society of Economic Geologists Newsletter*, 23(1), 9-13.

Wilde, S. A., Wu, F. Y., Zhao, G. C. (2010). The Khanka Block, NE China, and its significance for the evolution of the Central Asian Orogenic Belt and continental accretion. *Geological Society*, 388(1), 117-137.

Wu, F. Y., Jahn, B. M., Wilde, S. & Sun, D. Y. (2000). Phanerozoic Crustal Growth: U–Pb and Sr–Nd Isotopic Evidence from the Granites in Northeastern China. *Tectonophysics,* 328(1), 89-113.

Wu, F. Y., Sun, D. Y., Ge, W. C., Zhang, Y. B., Grant, M. L., Wilde, S. A. & Jahn, B. M. (2011). Geochronology of the Phanerozoic Granitoids in Northeastern China. *Journal of Asian Earth Sciences*, 41(1), 1-30.

Xue, J. L., Li, S. R., Sun, W. Y., Zhang, Y. Q. & Zhang, X. (2014). Characteristics of the genetic mineralogy of pyrite and its significance for prospecting in the Denggezhuang gold deposit, Jiaodong Peninsula, China. *Science China Earth Sciences,* 57(4), 644-661.

Yan, Y. T., Li, S. R., Jia, B. J., Zhang, N., Jiang, L. & Yan, L. N. (2012). Composition typomorphic characteristics of pyrite in various genetic type gold deposits. *Advanced Materials Research*, 463-464, 25-29.

Yaxley, G. M., Green, D. H. & Kamenetsky, V. (1998). Carbonatite metasomatism in the southeastern Australian lithosphere. *Journal of Petrology*, 39(11), 1917-1930.

Ying, J. F., Zhou, X, H., Li, S. R. & Sun, D. S. (2001). Genetic mineralogy of pyrite from Jindoushan gold deposit, Yantai, Shandong Province. *Chinese Journal of Geochemistry,* 20(3), 219-225.

Yuan, W. M., Mo, X. X., Yu, X. H. & Luo, Z. H. (1998). Reflections of gold mineralization from quartz in the Baijingou gold deposit, Eastern Kunlun Mountains (in Chinese with English abstract). *Bulletin of Mineralogy, Petrology and Geochemistry*, 17, 237-241.

Zeng, Q. D., Liu, J. M., Chu, S. X., Wang, Y. B., Sun, Y., Duan, X. X. & Zhou, L. L. (2012). Mesozoic molybdenum deposits in the East Xingmeng orogenic belt, northeast China: characteristics and tectonic setting. *International Geology Review*, 54(16), 1843-1869.

Zhai, D. G., Liu, J. J., Han, S. Y., Wang, J. P., Zhang, H. Y., Liu, Z. J, Yang, L. B., Zhang, H. F. & Lv, J. (2013). Typomorphic characteristics of pyrite and processes of changes and preservation of the Sandaowanzi Telluride-Gold Deposit in Heilongjiang Province (in Chinese with English abstract). *Acta Geologica Sinica*, 87(1), 81-90.

Zhang, Z. C., Mao, J. W., Wang, Y. B., Pirajno, F., Liu, J. L. & Zhao, Z. D. (2010). Geochemistry and geochronology of the volcanic rocks associated with the Dong'an Adularia–Sericite epithermal gold deposit, Lesser Hinggan Range, Heilongjiang Province, NE China: Constraints On the Metallogenesis. *Ore Geology Reviews*, 37(3), 158-174.

Zhao, H. D. (1990). A study on the pyroelectricity of pyrite and its application in gold prospecting (in Chinese with English abstract). *Acta Mineralogica Sinica*, 10(3), 278-284.

Zhao, Z. H. (1997). *Principle of trace element geochemistry* (in Chinese). Science Press, Beijing, 238pp.

Zheng, L., Gu, X. X., Zhang, Y. M. & Liu, R. P. (2013). Isotopic geochemistry and its implication to the genesis of Gaosongshan epithermal gold deposit in Heilongjiang Province, China (in Chinese with English abstract). *Acta Mineralogica Sinica*, 33(1), 101-109.

Zheng, L., Gu, X. X., Zhang, Y. M., Liu, R. P., Geng, H. Q., Wang, Y. Z., Zhao, H. H. & Li, Y. J. (2015). Element mobilization, mass-change quantification and formation mechanism of wall rock alteration in the Gaosongshan epithermal gold deposit, Heilongjiang Province, China (in Chinese with English abstract). *Geochimica,* 44(1), 87-101.

Zheng, L., Gu, X. X., Zhang, Y. M., Liu, R. P., Wang, J. L., Wang, Y. Z. & Zhao, H. H. (2014). Geological-geochemical characteristics and genesis of the Gaosongshan Gold Deposit in Heilongjiang Province, China (in Chinese with English abstract). *Bulletin of Mineralogy, Petrology and Geochemistry*, 33(5), 733-741.

Zhou, J. B., Wilde, S. A., Zhang, X. Z., Zhao, G. C., Zheng, C. Q., Wang, Y. J. & Zhang, X. H. (2009). The onset of Pacific margin accretion in NE China: evidence from the Heilongjiang high-pressure metamorphic belt. *Tectonophysics,* 478(3), 230-246.

Zhou, J. B., Wilde, S. A., Zhao, G. C., Zhang, X. Z., Zheng, C. Q., Wang, H. & Zeng, W. S. (2010). Pan-African Metamorphic and Magmatic Rocks of the Khanka Massif, NE China: further Evidence Regarding Their Affinity. *Geological Magazine*, 147(5), 737-749.

Zhou, T. H., Goldfarb, R. J. & Phillips, N. G. (2002). Tectonics and distribution of gold deposits in China-an overview. *Mineralium Deposita*, 37(3-4), 249-282.